PALEOCEANOGRAPHY, VOL. 12, NO. 3, PAGES 495-516, JUNE 1997

The late Cretaceous: Simulation with a coupled atmosphere-ocean general circulation model

Andrew B. G. Bush[1] and S. George H. Philander

Program in Atmospheric and Oceanic Sciences, Princeton University, Princeton, New Jersey

Abstract. Results are presented for the climate of the late Cretaceous period (~75–65 Ma) as simulated by a global climate model that is interactively coupled to a primitive equation global ocean model. Increased values of atmospheric CO_2 and altered land surface albedos are invoked to produce the warm Cretaceous temperatures that have been proposed from biogeographic reconstructions. For comparison, a control simulation of the present climate is performed. The globally averaged atmospheric temperature in the Cretaceous simulation stabilizes after 20 years of integration at a value that is 4°C greater than that of the present day. The lower troposphere in high latitudes contributes a majority of the globally averaged warming as a result of the elimination of the Antarctic and Greenland ice sheets. Nevertheless, equatorial surface temperatures are raised by ~5°C above those of the control simulation and offset somewhat the reduction in near-surface baroclinicity caused by the absence of the high-latitude ice sheets. In the Cretaceous simulation, global precipitation is approximately 10% greater than in the present day, with the only region of reduced precipitation occurring beneath the south Eurasian monsoon. Additionally, the amplitude of the seasonal cycle in near-surface temperatures is smaller in the Cretaceous and, in conjunction with increased mean annual temperatures, precludes the presence of any year-round snow or ice in the simulation. In high latitudes, however, there are regions that seasonally drop below freezing. The temperatures in these regions are warmer than have been previously observed in atmosphere-only simulations as a result of poleward heat transport by the ocean's surface currents.

1. Introduction

The mean annual temperature of the Cretaceous period was significantly warmer than that of the present day climate and was characterized by a 5°–15° poleward extension of tropical temperatures [e.g., *Smiley*, 1967; *Habicht*, 1979; *Savin*, 1977]. Evidence suggests that an increased level of CO_2, perhaps the result of increased tectonic activity, is the primary cause of the warm Cretaceous climate [*Sandberg*, 1983; *Berner*, 1991; *Cerling*, 1991]. Estimates of CO_2 amounts during the Cretaceous period range from as little as 3 times to as much as 10 times the present value [*Rau et al.*, 1989; *Lasaga et al.*, 1985]. It has consequently been proposed that no seasonal snow or ice existed in high latitudes during the Cretaceous. Atmospheric temperatures delivered from increased CO_2 experiments with general circulation models (GCMs) configured for the Cretaceous period, however, do not support the concept of a year-round snow- and ice-free planet [*Barron and Washington*, 1982, 1984, 1985; *Sloan and Barron*, 1990]. In fact, recent results indicate rapid fluctuations of sea level in response to Cretaceous glaciation [*Stoll and Schrag*, 1996]. The issue of freezing temperatures in high latitudes of the Cretaceous therefore remains an intriguing question in light of the discovery of Cretaceous flora and fauna in latitudes much higher than would be possible in today's climate [e.g., *Smiley*, 1967; *Brouwers et al.*, 1987] and one which should be investigated in a GCM which explicitly accounts for ocean dynamics.

Fluctuations in tropical temperatures of 3°–5°C around the present interglacial value have occurred throughout the planet's history [*Barron*, 1995]. Variations in the carbon cycle throughout the Phanerozoic [e.g., *Berner*, 1991], in conjunction with modeled CO_2-induced tropical temperature changes [e.g., *Manabe and Bryan*, 1985], support this link between tropical temperatures and atmospheric carbon dioxide. An

[1]Now at Department of Earth and Atmospheric Sciences, University of Alberta, Edmonton, Alberta, Canada.

Paper number 97PA00721.
0883-8305/97/97PA-00721$12.00

estimate of the mean Cretaceous temperature exceeds that of the present day by $\sim 3°-5°C$ near the equator and by $\sim 13°-30°C$ near the poles [*Barron*, 1983]. These numbers may at first suggest the existence of a so-called "equable" climate, one with little pole-to-equator temperature gradient and one which exhibits little seasonality. To date, however, general circulation models have had difficulty in delivering year-round polar warmth, particularly when large landmasses such as Eurasia, Pangaea, or Gondwanaland are located in high latitudes [respectively, *Sloan and Barron*, 1990; *Crowley et al.*, 1989; *Crowley et al.*, 1987]. Since near-surface temperature places an important constraint on the development and migration of life on the planet and can be dramatically altered by the presence of surface ocean currents, it is of general interest to explore the seasonal cycle of surface temperature in a model that can predict the impact of such currents. Additionally, what does an equable climate really mean for the atmosphere? Is the entire vertical structure of the atmosphere equable or can such a climate state exist only near the surface?

Our goal in the present study is to simulate the climate of the late Cretaceous through integration of a relatively high resolution coupled atmosphere-ocean general circulation model and to explore the seasonal behavior of the climate. (Of course, the verisimilitude of the model results depends both on the quality of the model itself and the accuracy of the proxy data with which the experiment has been designed; as will be demonstrated, the model results compare quite favorably with the available proxy data.) We also examine the tropical ocean currents and the wind-driven circulation which are forced by, and feed back on, such atmospheric conditions. Previous studies [*Barron and Peterson*, 1989, 1990; *Barron et al.*, 1981] have explored the mid-Cretaceous atmosphere and the mid-Cretaceous ocean individually in separate integrations. The dynamical variables delivered from such isolated integrations, however, will not be quite compatible with each other because atmosphere-ocean interaction is not included. Experiments with an atmospheric GCM coupled to a thermodynamic mixed layer ocean model have been performed to determine the impact of specified ocean heat transport on mid-Cretaceous climate [*Barron et al.*, 1993]. Representing the next evolutionary step in climate modeling, coupled atmosphere-ocean models are becoming increasingly useful for studies of both the present-day climate [e.g., *Philander et al.*, 1995] and paleoclimate [*Manabe and Stouffer*, 1995].

A paleobiogeographic reconstruction of the continental configuration of the late Cretaceous [after *Ziegler et al.*, 1984] is employed to construct the continental grid that is imposed in the numerical model (Figure 1). The salient features are (1) the Tethys Ocean (bounded by the continents of North and South America, Eurasia, and Africa), (2) the separation of North and South America which provides an oceanic gateway between the Tethys Ocean and the Pacific, (3) the separation of Africa and Asia (with the Tethys Seaway running between them), (4) the Indian subcontinent is an island in the southern subtropics, and (5) the Australian continent is attached to Antarctica. We will demonstrate that all of these features have important climatic consequences on the atmosphere-ocean system.

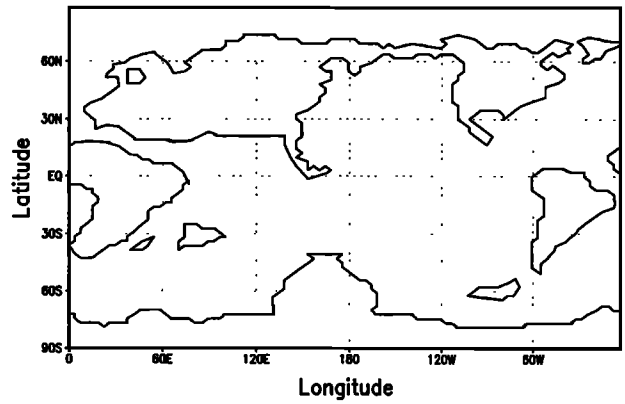

Figure 1. The continental configuration employed in the Cretaceous experiment.

This paper begins with descriptions of the atmospheric and oceanic models and the coupling strategy (section 2). Presentation of the results (section 3) is followed by a discussion (section 4) and conclusions (section 5).

2. Description of the Models and the Coupling Scheme

The atmospheric component of the coupled model is GFDL's (Geophysical Fluid Dynamics Laboratory) spectral climate model [*Gordon and Stern*, 1982]. To the spherical harmonic decomposition of the state variables we apply rhomboidal truncation at wavenumber 30. The equivalent Gaussian grid has a resolution of 2.25° in latitude and 3.75° in longitude. There are 14 unevenly spaced σ-levels in the vertical (where σ, a normalized pressure coordinate, is defined by $\sigma = P/P^*$ with P^* equal to the spatially varying surface pressure). The σ-levels are given by $\sigma = 0.015$, 0.05, 0.101, 0.171, 0.257, 0.355, 0.46, 0.568, 0.676, 0.777, 0.866, 0.935, 0.979, and 0.997. In many of the results to be shown, quantities are shown on the lowest model level ($\sigma = 0.997$) and are referred to as "near-surface" quantities. For a standard atmosphere this level corresponds to approximately 30 m above ground.

Distribution of the continents is specified in the model as shown in Figure 1. During the integration, surface land temperatures are calculated under the restriction of no surface heat storage after taking into account the value of the surface albedo, the net flux of solar and terrestrial radiation, and the fluxes of sensible and la-

tent heat. Spatially varying surface albedos are initially specified at each (equivalent) grid point but may subsequently be modified over land during the integration if snow cover is present. Ocean albedos on the equator are given a value of 0.06; in higher latitudes this value is modified by the calculated solar zenith angle. Present-day values of surface albedo are imposed over the land in the tropics and in midlatitudes. In high latitudes above 60°N and below 60°S, land albedos are assigned a snow-free value of 0.2, a value that is typical in upper midlatitudes in the present-day and was chosen to reflect the fact that in the Cretaceous, vegetation had spread into the northern regions that are presently ice-covered [e.g., *Brenchley*, 1984]. Soil moisture is calculated by the conceptually simple bucket scheme with a capacity of 15 cm. A moist convective adjustment scheme [*Stone and Manabe*, 1968] is employed to predict precipitation. As the locations of coastal river outlets in the late Cretaceous are unknown to us, we neglect the contribution of continental runoff to the freshwater flux entering the ocean in this initial study. Such runoff would impact regional surface salinity near the mouths of the major Cretaceous rivers. Clouds are predicted according to the scheme detailed by *Wetherald and Manabe* [1988]. The solar constant has not been changed in this experiment and has a value of 1356 W/m^2 [*Kondratyev*, 1969]. Insolation is seasonally (and not diurnally) varying, and present-day orbital parameters are imposed.

The spatially uniform mixing ratio of CO_2 in the atmosphere is increased (at the outset of the integration) by quadrupling its present value of 300 ppm. This value for the late Cretaceous CO_2 mixing ratio remains on the lower end of the hypothesized values (see the Introduction), since the late Cretaceous, although much warmer than present, was cooler than the mid-Cretaceous [*Wolfe and Upchurch*, 1987; *Parrish and Spicer*, 1988]. The distribution of ozone varies with latitude, height, and season, and for lack of ozone data during the Cretaceous, we do not change its distribution from that of the present climate. Although high topographic features such as the Himalayas, the Alps, and much of the Rockies were formed after the Cretaceous period, other topographic features were present. For lack of specific topographic height data, however, we make the simplification of imposing flat continents (and therefore gravity wave drag is also set to zero). High Cretaceous topography, however, would alter the regional circulation and precipitation patterns; we discuss this caveat to our results when appropriate.

The oceanic component of the model is GFDL's modular ocean model, a three-dimensional primitive equation general circulation model whose origins may be traced to *Bryan* [1969] and whose details are given by *Pacanowski et al.* [1991]. The model employs a finite difference representation of variables with a ∇^4 horizontal diffusion operator and, since the model domain is global, additional smoothing is required in high latitudes where grid boxes converge. Vertical mixing is based on a Richardson number scheme developed by *Pacanowski and Philander* [1981]. A horizontal resolution of 2° in latitude and 3.62° in longitude is chosen so as to be nearly equal to the equivalent spatial grid of the spectral atmospheric model. Fifteen unevenly spaced levels in the vertical are specified with the grid box centers located at depths of 15, 52, 104, 180, 289, 441, 648, 924, 1279, 1724, 2264, 2898, 3620, 4416, and 5265 m. Note that higher vertical resolution is realized in the upper 500 m in order to more accurately capture the wind-driven circulation. Coastlines are imposed according to the late Cretaceous geometry shown in Figure 1. As a simplification, bathymetry is neglected and a uniform ocean depth of 5700 m is imposed (in both the Cretaceous and control simulations). A further simplification in this study is that we do not incorporate any shallow epicontinental seas, which were at a relatively low areal extent in the late Cretaceous [*Brass et al.*, 1982]. We discuss this caveat in section 4.

The atmosphere and ocean models are dynamically and thermodynamically coupled and are time-integrated asynchronously with a 1-day integration interval. Boundary condition data from one model are spatially interpolated for input onto the grid of the second model (although the grid spacings are nearly equal in the two models). Variables which are input as boundary conditions for the atmospheric model are sea surface temperature and surface current velocities. Boundary conditions delivered from the atmospheric model for input into the ocean model are vector components of wind stress, net heat flux, net freshwater flux, and net shortwave radiation.

The initial condition of the ocean is specified to be one of rest with temperature and salinity profiles that vary in the vertical and meridional directions. In the absence of dynamics it is the incoming radiative forcing which determines the meridional structure of the ocean's surface temperature. When dynamics are introduced, this zonally invariant state will be perturbed by the meridional flows induced by the presence of continental barriers. Since we impose present-day insolation, the meridional structure of the ocean that is consistent with such radiative forcing is taken to be the zonal mean of present-day temperature and salinity as determined from *Levitus* [1982]. Although such an approach is consistent for the present-day orbital parameters that we have imposed, it is possible that these parameters in the Cretaceous may have been quite different from today; we discuss this caveat in section 4.

Given existing computational constraints which preclude a spin-up of the deep ocean currents, our primary interest in the present study is therefore to establish seasonal climatologies for the atmosphere, the equatorial ocean, and the extratropical upper ocean. Since the

wind-driven ocean circulation takes of order 10^0-10^1 years to spin up, the coupled model is integrated for a duration of 32 years, during which no flux correction is applied. These simulations are of sufficient duration for the achievement of thermal equilibration of sea surface temperature to the increased radiative forcing and for the genesis of major ocean currents such as equatorial jets and gyre circulations with their heat-transporting western boundary currents. In the remaining figures in this paper, monthly mean quantities have been averaged over the last 6 years of the integration, a period over which the global mean temperature is relatively stable (see Figure 2).

The coupled model employed for the control simulation of the present-day climate is identical to that described above for the Cretaceous with the following exceptions. We specify the current continental positions, albedos, and continental topographic heights (which have been spectrally smoothed to be consistent with the spectral truncation employed in the model). Gravity wave drag is included over the higher topographical features and a CO_2 mixing ratio of 300 ppm is specified. We will hereafter refer to quantities delivered by the control run as "present-day" quantities.

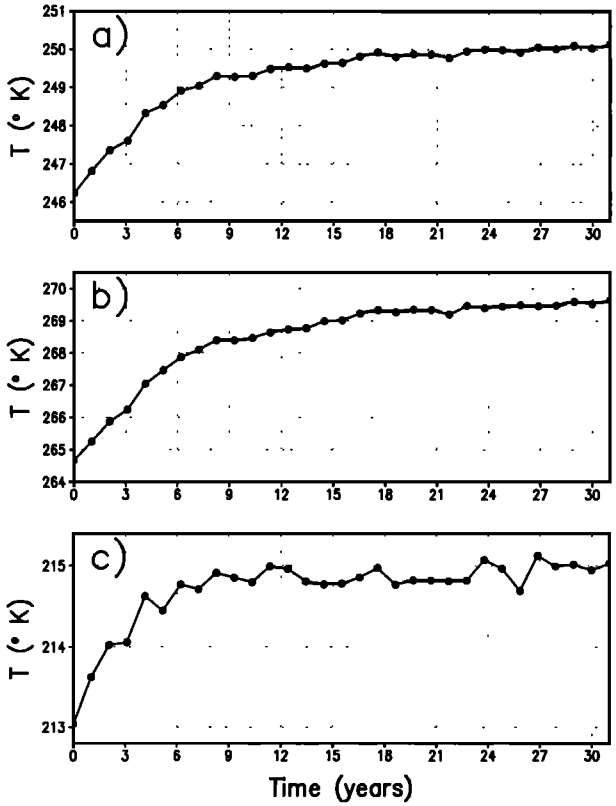

Figure 2. Annual mean temperature as a function of time (in years) for the Cretaceous simulation. (a) global average, (b) tropospheric average, and (c) stratospheric average (where the mean tropopause is taken as the $\sigma = 0.257$ surface).

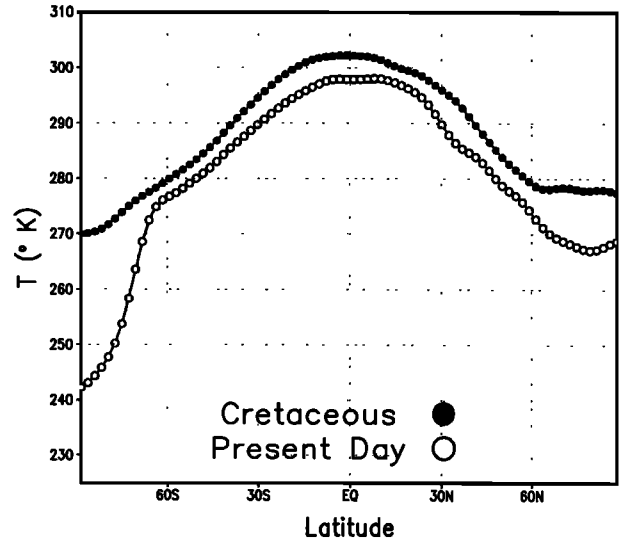

Figure 3. Annual and zonal mean near-surface temperature (in kelvins) for the Cretaceous (open circles) and present day (solid circles) as a function of latitude.

3. Climate of the Late Cretaceous

This section presents a side-by-side comparison of the results from the late Cretaceous simulation and from the present-day simulation. For convenience, this section is divided into subsections according to the relevant diagnostic quantity.

3.1. Atmospheric Temperature

The time evolution of global atmospheric temperature (Figure 2a) indicates the response time of the model atmosphere (with respect to its isothermal initial conditions) to the Cretaceous forcing parameters which we impose. The response of the model atmosphere to quadrupled CO_2 is rapid over the first 10 years of the integration (as also seen in the increased CO_2 experiments of *Washington and Meehl* [1984]). A less rapid thermal response is evident over the next 10 years as the high-latitude wind-driven circulation begins to equilibrate. After 20 years the global temperature remains fairly uniform, indicating that at the end of the integration period the atmosphere is in a state of quasi-equilibrium with the underlying ocean (whose sea surface temperature (SST) provides the dominant atmospheric forcing). The global mean temperature at the end of the integration is ~4°K greater than that of the present day. Decomposition into tropospheric (Figure 2b) and stratospheric (Figure 2c) components reveals that the dominant thermal response occurs in the troposphere, where mean temperatures increase 5°K above the isothermal initial condition temperature.

Comparison of the near-surface zonal mean temperature as a function of latitude in the two simulations (Figure 3) indicates that the largest amount of sur-

face warming in the Cretaceous occurs in the high latitudes of both hemispheres. In the high northern latitudes, a warming of 18°–20°K occurs, whereas in the high southern latitudes an even more drastic warming of 30°–35°K is indicated. These warm high-latitude Cretaceous temperatures are a result of the absence of the permanent Greenland and Antarctic ice sheets and their concomitant ice-albedo feedback. Cretaceous surface temperature at the equator has a value of 302°K (~5°K greater than in the present-day simulation) with a smaller warming in midlatitudes (~2°–3°K).

The spatial distribution of annual mean surface temperature in the Cretaceous (Figure 4a) reveals that the highest temperatures are found over the northern re-

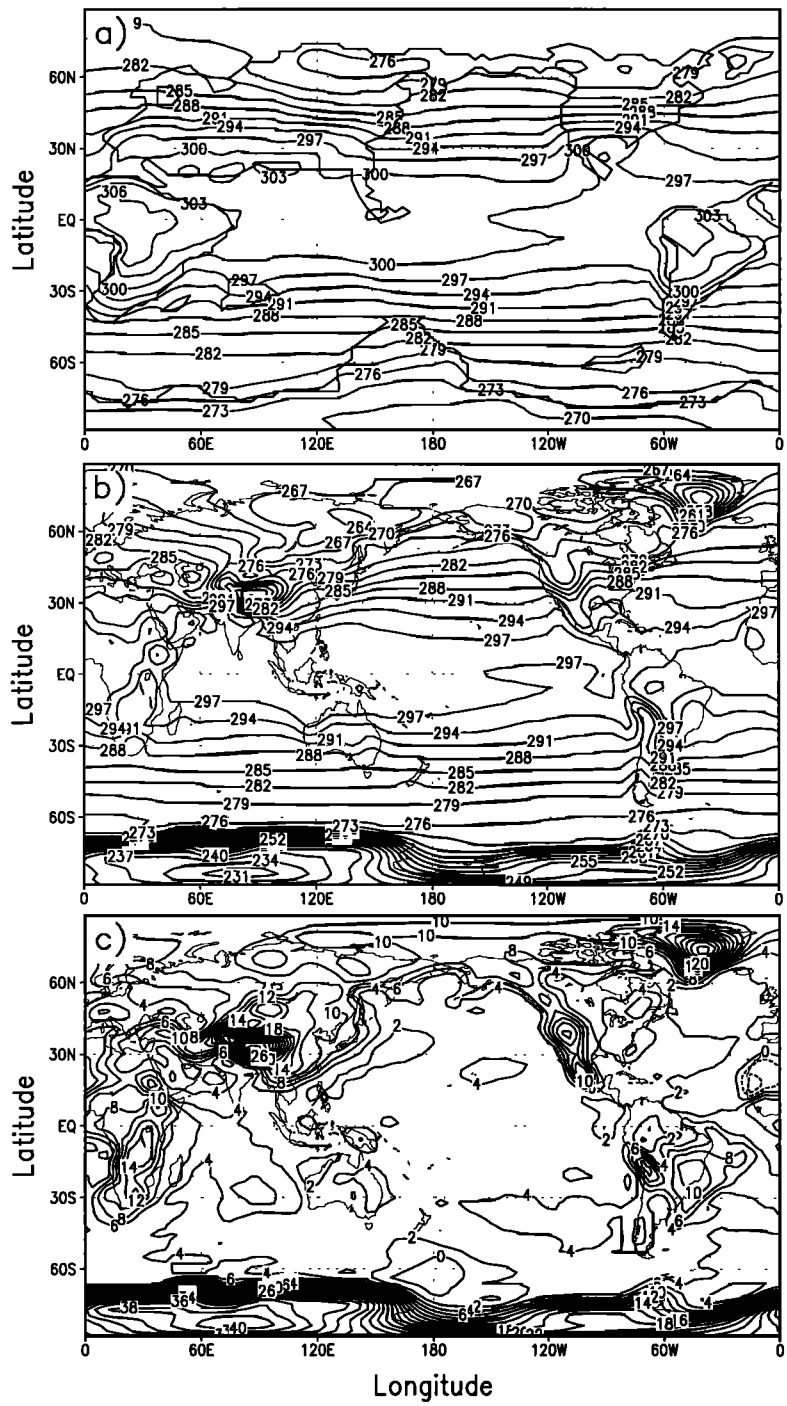

Figure 4. Annual mean near-surface ($\sigma = 0.997$) temperature as a function of longitude and latitude for (a) the Cretaceous, (b) the present day, and (c) their difference (Cretaceous minus present day). The contour intervals are 3°K in Figures 4a and 4b and 2°K in Figure 4c.

gions of the African continent, with typical values reaching 307°K (Figure 4a). There is a poleward expansion of 10°–15° of tropical temperatures (compare the 297°K isotherm in Figures 4a and 4b), and the annual mean temperature is above freezing everywhere but near the south pole. Annual mean temperatures of a few degrees below freezing in southern Australia during the Cretaceous have been suggested by *Rich et al.*, [1988] and agree well with the results presented here. Fossil records from the North Slope of Alaska indicate that dinosaurs roamed the high paleolatitudes of North America [*Brouwers et al.*, 1987], indicating that at least in the annual mean the surface temperature should be above zero. In this simulation the annual mean temperature in this region is approximately 6°C (Figure 4a).

Despite the warm annual mean temperatures, however, there is still a seasonal cycle with which the flora and fauna of the time would have had to contend. The seasonal cycle can plunge certain regions below freezing, thereby precluding the year-round existence of species intolerant to freezing temperatures. (This does not, however, preclude the possibility of seasonal migration.) The annual mean near-surface temperature is shown by contours in Figure 5. In the grey scale is given the amplitude of the seasonal cycle in temperature; that is, for the northern hemisphere, the actual July temperature at a given location is the sum of the annual mean (contour) plus the amplitude of the seasonal cycle (shaded), and in January the temperature is the annual mean minus the amplitude of the seasonal cycle. The bold contour denotes the freezing line poleward of which temperatures seasonally drop below freezing. It is evident from the figure that the amplitude of the seasonal cycle in the Cretaceous is much smaller than in the present day. Through their feedback on albedo, seasonal snow and ice induce large variations in seasonal

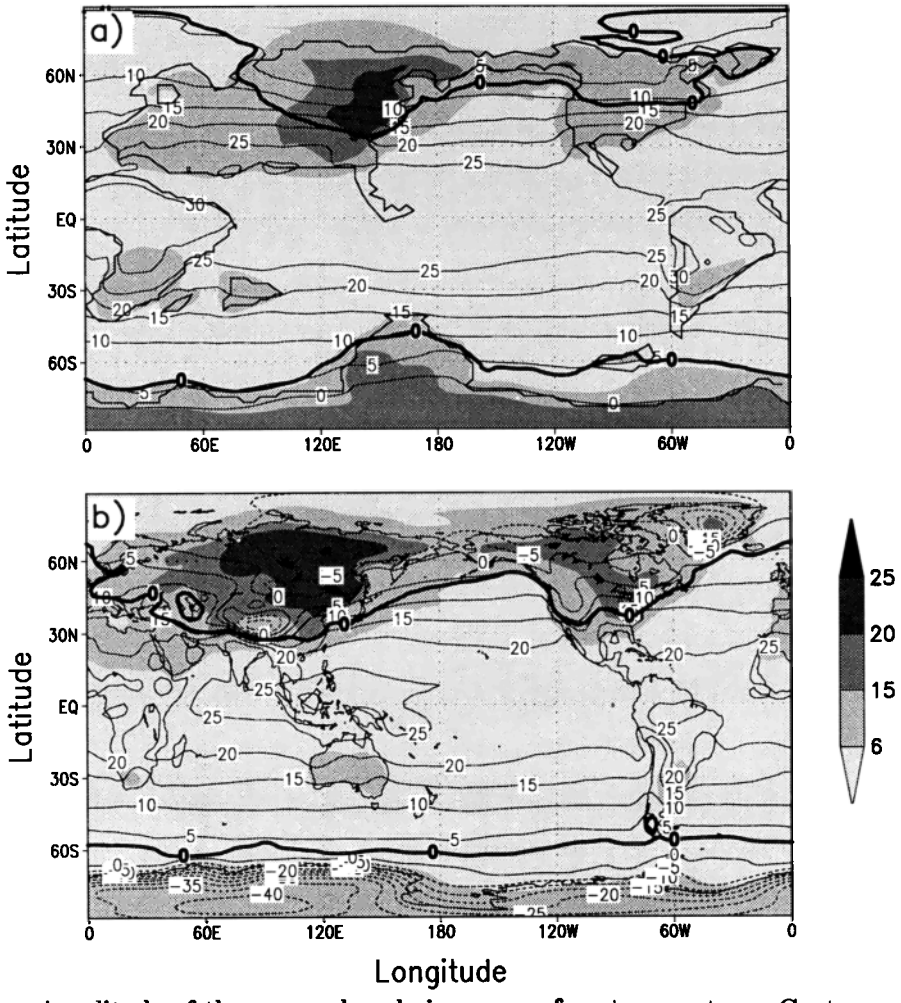

Figure 5. Amplitude of the seasonal cycle in near-surface temperature. Contours show the annual mean near-surface ($\sigma = 0.997$) temperature (contour interval 5°K) for the (a) Cretaceous and (b) present-day climates. The shaded values are the amplitude of the seasonal cycle (see text for definition). The bold line is the freezing line (poleward of this line the seasonal temperature drops below freezing).

temperature. The reduced areal extent of snowfall in the Cretaceous leads to a weaker seasonal cycle in the continental interiors. The freezing line has shifted poleward by roughly 10°, and freezing temperatures are absent over a very large portion of western Eurasia. These warm western European temperatures are due in part to the subtropical diversion around the northern rim of Africa of a westward circumglobal tropical current (see section 3.6).

The vertical structure of the annual and zonal mean temperature and zonal velocity fields (Figure 6) demonstrates that the absence of the Greenland and Antarctic ice sheets causes a reduction in the equator-to-pole temperature gradient in the lower troposphere (although this is somewhat offset by the rise in equatorial temperatures). Middle to upper tropospheric temperature gradients, however, are comparable to those of the present day. Hence there is little reduction in strength of the upper tropospheric geostrophic winds in midlatitudes. In fact, the core jet speeds in the Cretaceous simulation are stronger than those in the control simulation (this was also observed in the atmosphere-only simulation of *Barron and Washington* [1982]). There are three factors contributing to the increased jet strength in the Cretaceous simulation. In the northern hemisphere the zonal surface winds are stronger (as a result of no topographical barriers) and the midlatitude baroclinicity above the boundary layer is comparable to that of the control run. Through geostrophy this results in stronger upper tropospheric winds. Another factor affecting the strength of the jets is topographic gravity wave drag, which reduces jet speeds in the control simulation but is absent in the Cretaceous experiment since there are no mountains in this experiment. A third factor affecting the large-scale winds is the increased moisture content and latent heat release in the Cretaceous atmosphere, factors that will be explored in more detail (sections 3.3 and 3.4).

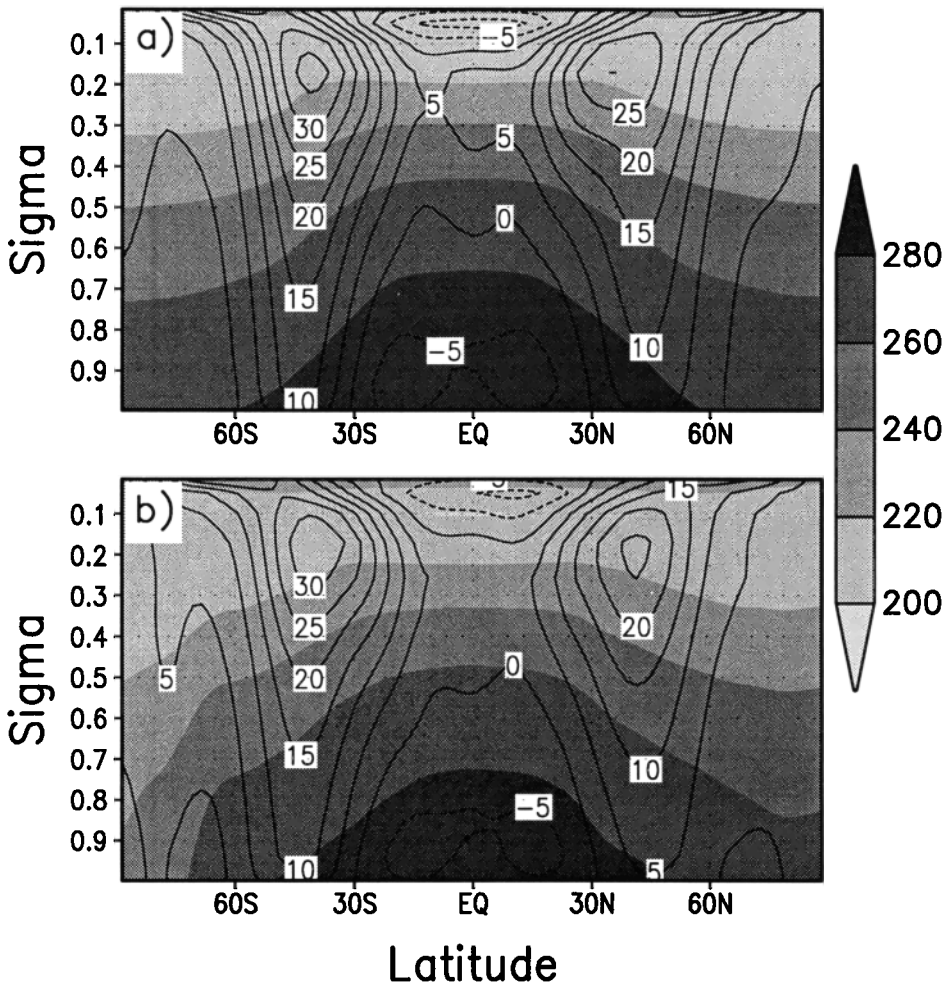

Figure 6. Vertical profile of annual mean temperature (shaded) and zonal velocity (contours) as a function of latitude for (a) the Cretaceous and (b) the present day. Contour intervals are 20°K for temperature and 5 m/s for zonal velocity.

Evident from Figure 6, and also from the atmospheric simulation of *Barron and Washington* [1982], is the fact that the midlatitude jets in an ice-free environment are not displaced poleward, as was hypothesized by *Luyendyk et al.* [1972] when performing biogeographical reconstructions. Figure 6 also demonstrates that the equatorial upper tropospheric westerlies and surface easterlies are stronger. These features are signatures of a stronger Pacific Walker circulation which will be diagnosed explicitly in the following section. The spatial pattern of the surface winds has important implications for the wind stress that drives the surface currents of the oceans (see section 3.6) [*Bush*, 1997].

3.2. Hadley and Walker Circulations

Since large-scale atmospheric circulations play a fundamental role in the spatial deposition of observables such as coal and evaporites, we diagnose in this section the mean meridional and mean zonal flows as described by the Hadley and Walker circulations, respectively. The Hadley circulation Φ is computed from the zonally averaged meridional velocity $\overline{V}$ according to

$$\frac{\partial \Phi}{\partial p} = \frac{2\pi R \cos\phi}{g}\,\overline{V}, \tag{1}$$

where R is the Earth's radius, g is gravitational acceleration, ϕ is latitude, and p is pressure. We assume that $\Phi = 0$ at the top of the model atmosphere and integrate 3.1 in the vertical to determine Φ. Note that this method is equivalent to solving the (more correct) Poisson equation $\nabla^2\Phi = \zeta$ (where ζ is the x component of vorticity) if the mean divergence of the zonally averaged flow is zero, a constraint that is quite well satisfied in the model.

The annual mean Hadley circulation for the Cretaceous and for the present day (Figures 7a and 7b, respectively) indicate a general reduction in strength of the southern hemisphere cells in the Cretaceous, with the south equatorial Hadley cell weakening by 20%. (The sign convention is such that a negative value indicates counterclockwise motion in the diagram.) Subsidence in the high southern latitudes decreases dramatically in the Cretaceous in response to the elimination of the Antarctic ice sheet, which in the present climate induces strong subsidence poleward of 75°S. In consequence, the strengths of the middle and high-latitude cells decrease. The north equatorial Hadley cell, on the other hand, is ~20% stronger. The general pattern is one of weakening of the southern hemisphere cells and strengthening of the northern hemisphere cells.

The largest change, however, is in the annual mean position of the intertropical convergence zone (ITCZ), which is evident in Figure 7 as the region of surface convergence between the two strong equatorial cells. In the present-day simulation, the annual mean ITCZ is located in the northern hemisphere at ~ 7°N over the warm waters associated with the North Equatorial Countercurrent (NECC). The NECC, however, is absent in our Cretaceous simulation as a result of the open continental geometry of the western Pacific. In addition, separation of the North and South American continents allows stronger northeasterly trades to flow from the Tethys basin into the Pacific basin, whereas the strength of the southeasterly winds off the western coast of South America remain approximately the same. The ITCZ between these two air masses is consequently displaced southward in the Cretaceous. There is a concomitant equatorward shift from 36°N to 30°N of the northern subtropical high (the region of surface divergence between the north equatorial cell and the northern midlatitude cell of Figure 7). From evaporite deposits *Gordon* [1975] has noted such an equatorward shift of the subtropical high during the Mesozoic.

The Walker circulation Ψ is diagnosed in a similar fashion to the Hadley circulation after meridionally averaging the zonal velocity component U between 30°S to 30°N. We assume $\Psi = 0$ at the surface and vertically integrate

$$\frac{\partial \Psi}{\partial p} = \frac{2\pi R}{g}\,\overline{U}, \tag{2}$$

where the constants are defined as in (1). (Note from Figure 7 that between 30°S and 30°N the mean divergence of flow in the x–z plane averages nearly to zero so that this method is a good approximation to solving the Poisson equation $\nabla^2\Psi = \eta$, where η is the y component of vorticity.)

The annual mean Walker circulation for the Cretaceous and for the present day (Figures 8a and 8b, respectively) indicate a striking ~15% increase in strength of the Pacific Walker cell in the Cretaceous. (The sign convention in Figure 8 is such that a positive value along a closed contour indicates clockwise motion in the diagram.) In addition, the Cretaceous Pacific cell has a greater zonal extent as a result of the wider Pacific basin. The increased strength of the cell is caused in part by an increase in latent heat release during tropical convection over the very warm western Pacific SST (see section 3.6). The increased heat release, which may be attributed to the increased moisture content of the atmosphere in the warmer Cretaceous climate, fuels stronger convection with concomitant increases in upper level divergence and lower level convergence. The enhanced Pacific Walker circulation results in stronger upper tropospheric westerlies and stronger lower tropospheric easterlies over the tropical Pacific (see Figure 6).

3.3. Precipitation

Variations in the position and strength of zones of convergence and divergence, as reflected in a mean sense

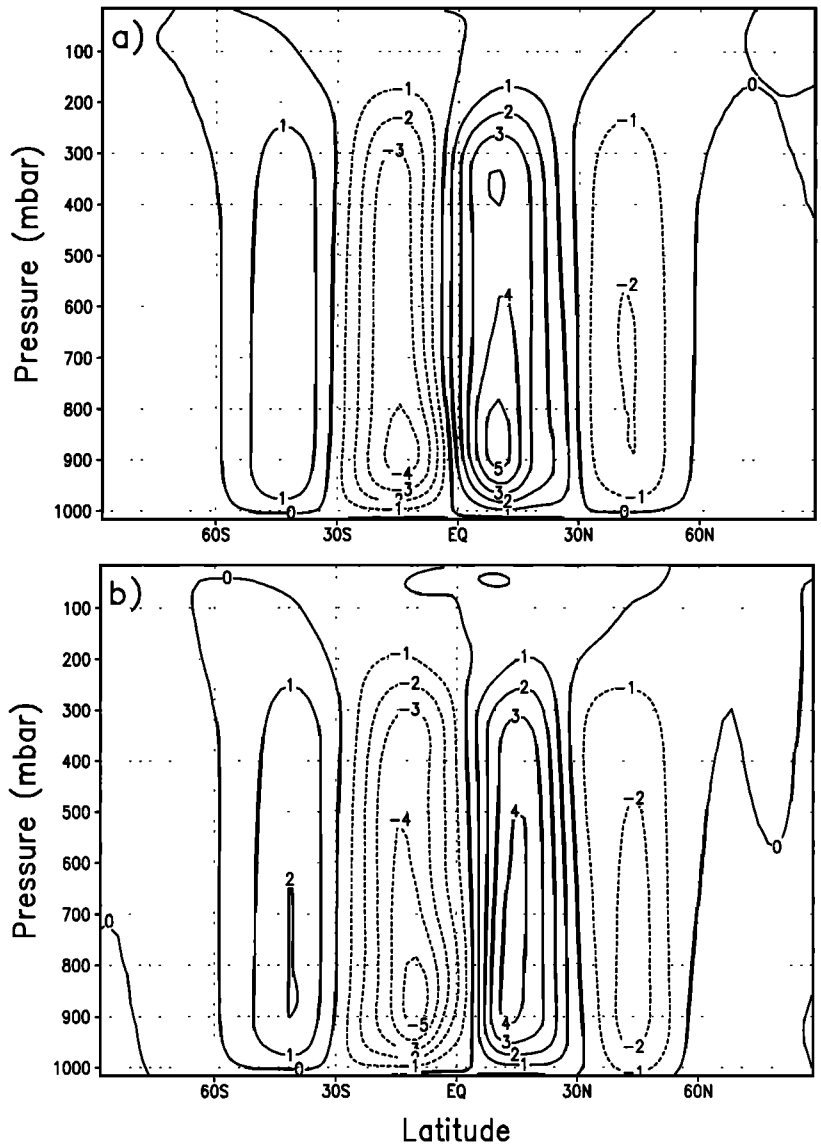

Figure 7. Annual mean Hadley circulation ($\times 10^{10}$ kg/s) for (a) the Cretaceous and (b) the present day. Contour interval is 10^{10} kg/s, and the sign convention is such that a negative value indicates counterclockwise flow in the plane of the diagram.

by variations in the Hadley and Walker circulations, will directly impact the patterns of precipitation and buoyancy forcing of the oceans. Annual mean precipitation rates for the Cretaceous and for the present day (Figures 9a and 9b, respectively) reveal a broad increase in annual mean precipitation in both the tropics and midlatitudes in the Cretaceous. Globally averaged values of annual mean precipitation for the Cretaceous and for the present-day simulations are 0.97 m/yr and 0.88 m/yr, respectively, indicating a 10% increase in the warmer climate. Rainfall rates under the northern midlatitude jet are substantially higher over Cretaceous North America than in the present, with values exceeding 0.35 cm/d over much of the continent from 40°–55°N. *Broccoli and Manabe* [1992] have demonstrated that increased precipitation over continental interiors is consistent with the absence of topography (for the modern configuration of topography); the simulated increase in continental precipitation may therefore not be as large if approximate Cretaceous topography were included. Annual mean precipitation is enhanced over northern and eastern Africa in the Cretaceous (especially over the region that is currently the Sahara Desert), an enhancement that reflects both the geographical positioning of this region underneath the ITCZ and weaker subsidence from the Walker circulation (see Figure 8a).

During the northern summer months of June-July-August (JJA), precipitation in the present-day simulation is dominated by the south Asian monsoon (Fig-

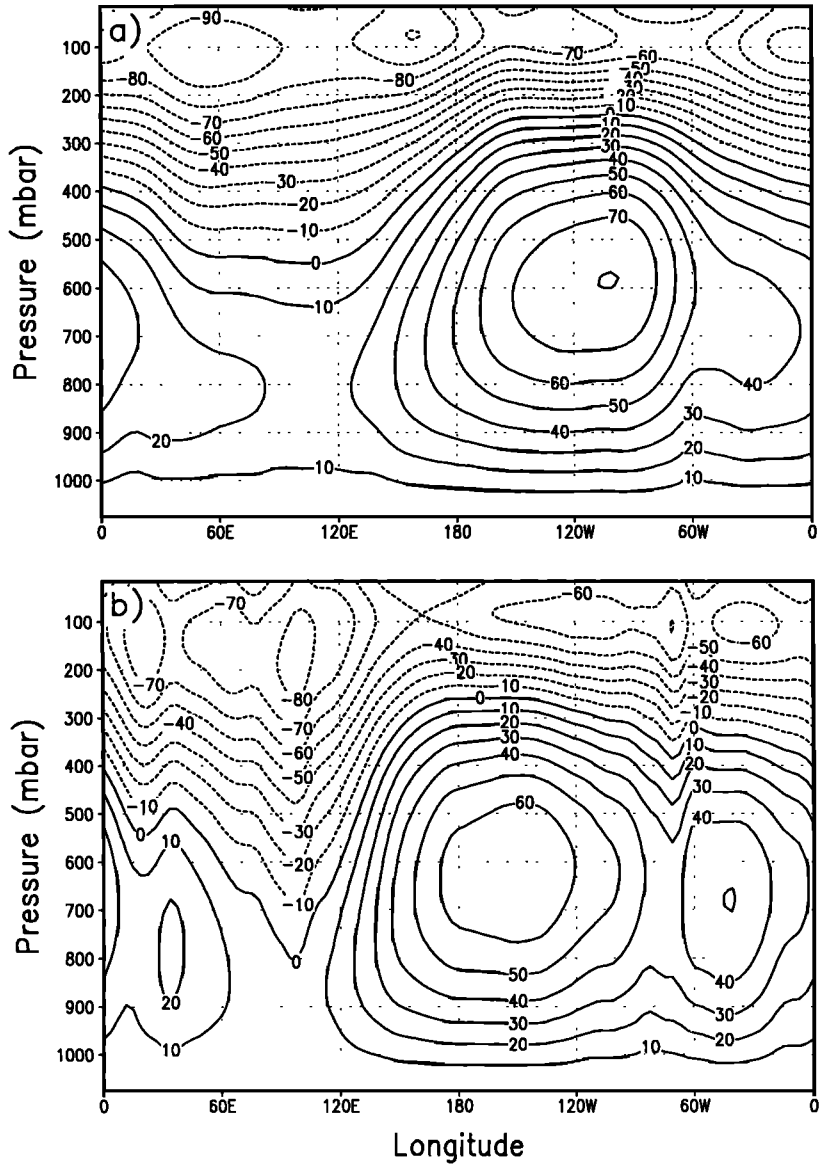

Figure 8. Annual mean Walker circulation ($\times 10^{10}$ kg/s) for (a) the Cretaceous and (b) the present day. Contour interval is 10^{11} kg/s, and the sign convention is such that a positive value indicates clockwise flow around a closed streamline.

ure 9d), with simulated precipitation rates regionally exceeding 2.2 cm/d. In the south Eurasian region of the Cretaceous, there is a fairly uniform ~1 cm/d rate of precipitation (Figure 9c). This reduced rate of precipitation is the result of a weaker monsoon circulation in the Cretaceous (see section 3.5). As a result of increased surface temperatures and convection during the southern summer months of December-January-February (DJF), mean precipitation over South America during the Cretaceous exceeds its present value by 66% in some regions. During these months the maximum rainfall can exceed 2.1 cm/d. In the Cretaceous, DJF rainfall rates over southeastern Africa and JJA rates over northwestern coastal Africa can both exceed 1.5 cm/d, a value that is competitive with the simulated precipitation rates in the present-day monsoon.

Zonal mean rates of precipitation as a function of latitude for the Cretaceous (Figure 10a) and for the present day (Figure 10b) reveal that the equatorial peak in annual mean precipitation (indicative of the mean location of the ITCZ) is nearer to the equator in the Cretaceous. In general, there is a 0.05–0.1 cm/d increase in mean Cretaceous precipitation in both the tropics and midlatitudes. One exception, however, is the JJA equatorial peak, which is smaller in the Cretaceous by ~0.06 cm/d as a result of a weaker south Eurasian monsoon (see Figure 9c). The increased midlatitude precipitation in the Cretaceous simulation implies an increase in

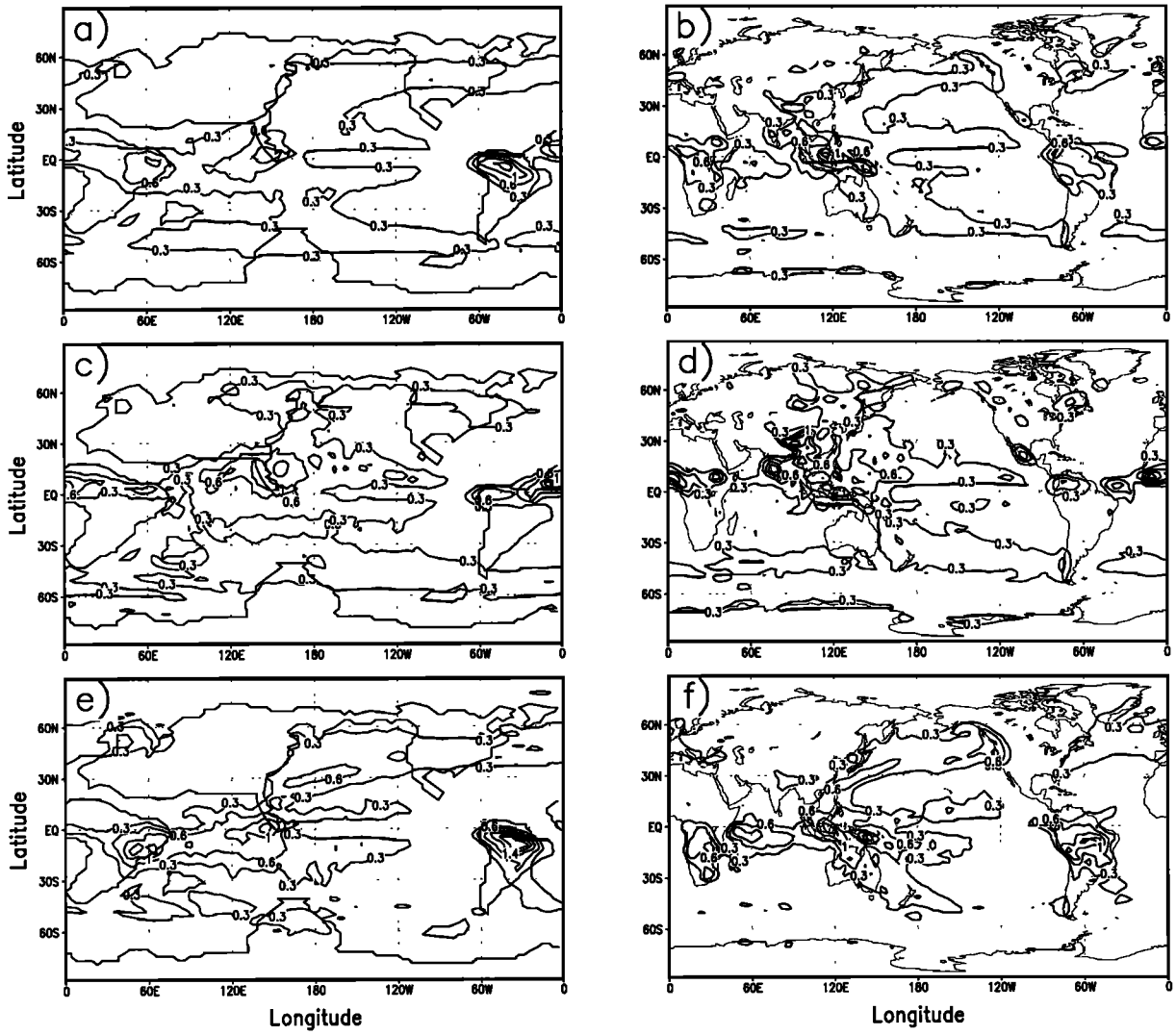

Figure 9. Spatial distribution of the annual mean precipitation (in centimeters per day) for (a) the Cretaceous and (b) the present day. Also shown are the JJA averages (c) and (d) and the DJF averages (e) and (f) . Contours in all panels are at 0.3, 0.6, 1, 1.4, and 1.8 cm/d.

the midlatitude flux of latent heat, as demonstrated in the enhanced CO_2 experiments of *Manabe and Bryan* [1985]; this impacts the heat transport, as will be shown in the next section.

3.4. Mean Winds and Heat Transport

Section 3.2 demonstrated that there are significant differences in the large-scale atmospheric circulation of the Cretaceous atmosphere compared with that of the present day. An elongated and strengthened Pacific Walker cell dominates the zonal equatorial circulation, whereas weaker southern and stronger northern Hadley cells dominate the mean meridional circulation. These differences are consequences of the adjustment of the large-scale flow to the altered boundary forcing provided by the Cretaceous environment. Annual mean zonal and meridional velocities in the lowest model level ($\sigma = 0.997$) for the Cretaceous (Figures 11a and 11b, respectively) and for the present day (Figures 11c and 11d, respectively) reveal that the south Eurasian monsoon westerlies are not as strong in the Cretaceous and do not dominate the easterly trades in the annual mean as they do in the present day. Local regions of westerlies exist on the equator on the western coasts of Africa and South America in both simulations; these westerlies are induced by the semiannual cycle of equatorial land heating by solar radiation.

Low-level westerlies in the northern midlatitudes of the Cretaceous are stronger by ~2 m/s as a result of the absence of topographical barriers and the eddies that such barriers can induce. Low-level easterlies over the tropical Pacific Ocean are ~2 m/s stronger and reflect the stronger Pacific Walker cell. A salient feature of

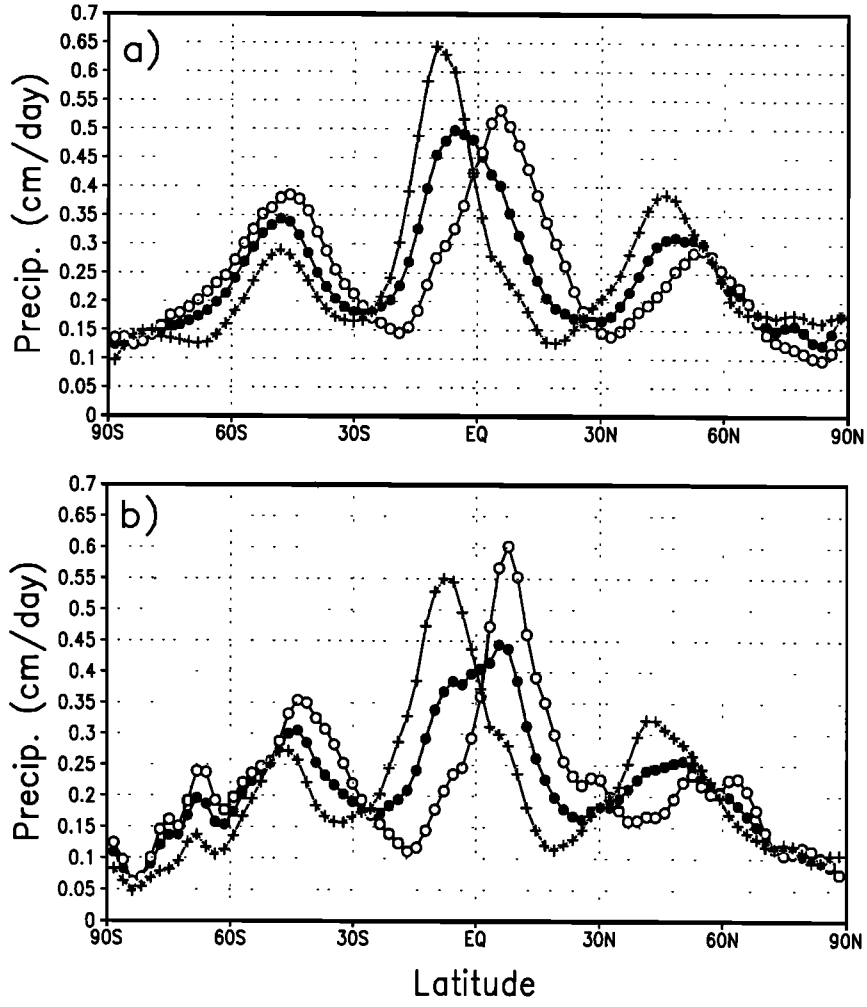

Figure 10. Zonal mean precipitation rate (in centimeters per day) for (a) the Cretaceous and (b) the present day. In each panel are shown the annual mean (solid circle), the JJA mean (open circles), and the DJF mean (crosses).

Figure 11a is that the easterly trade winds have a much larger magnitude over the eastern Pacific in the Cretaceous as a result of the separation of North and South America. These winds are not moderated by Central American heating and surface drag as they are in the present day (Figures 11b and 11d) and have a sufficiently strong northerly component to prevent northward displacement of the ITCZ by the southeasterly winds off the western coast of South America (Figure 11c).

The upper tropospheric (σ=0.355) wind components for both simulations (Figure 12) show that at this level the midlatitude jets have comparable maximum core speeds, although the geographical locations of these maxima are not the same. These differences result from variations in the topographic and continental forcing of stationary planetary waves. For example, in the northern hemisphere jet the maximum speed in the Cretaceous is over North America, whereas in the present day the Rockies induce downstream eddy activity which weakens the mean zonal flow of the jet and increases the mean meridional flow (Figures 12b and 12d). The intensified Pacific Walker circulation of the Cretaceous is evident as stronger equatorial westerlies (compare Figures 12a and 12b). The mean meridional velocities of the Cretaceous (Figure 12c) reflect the symmetry around the equator of the Hadley circulation (especially over the western Pacific) as well as the lack of topographically induced eddies over North America and central Eurasia.

The net poleward heat transport of the atmosphere may be described by $\overline{V'T'}$ (where an overbar indicates a time average (which we take to be the annual mean) and a prime indicates a deviation from that average; see *Peixoto and Oort* [1992]). The annual mean, vertically and zonally averaged $\overline{V'T'}$ as a function of latitude (Figure 13) reveals large equatorward heat fluxes at 10°S and 13°N which are produced by strong equator-

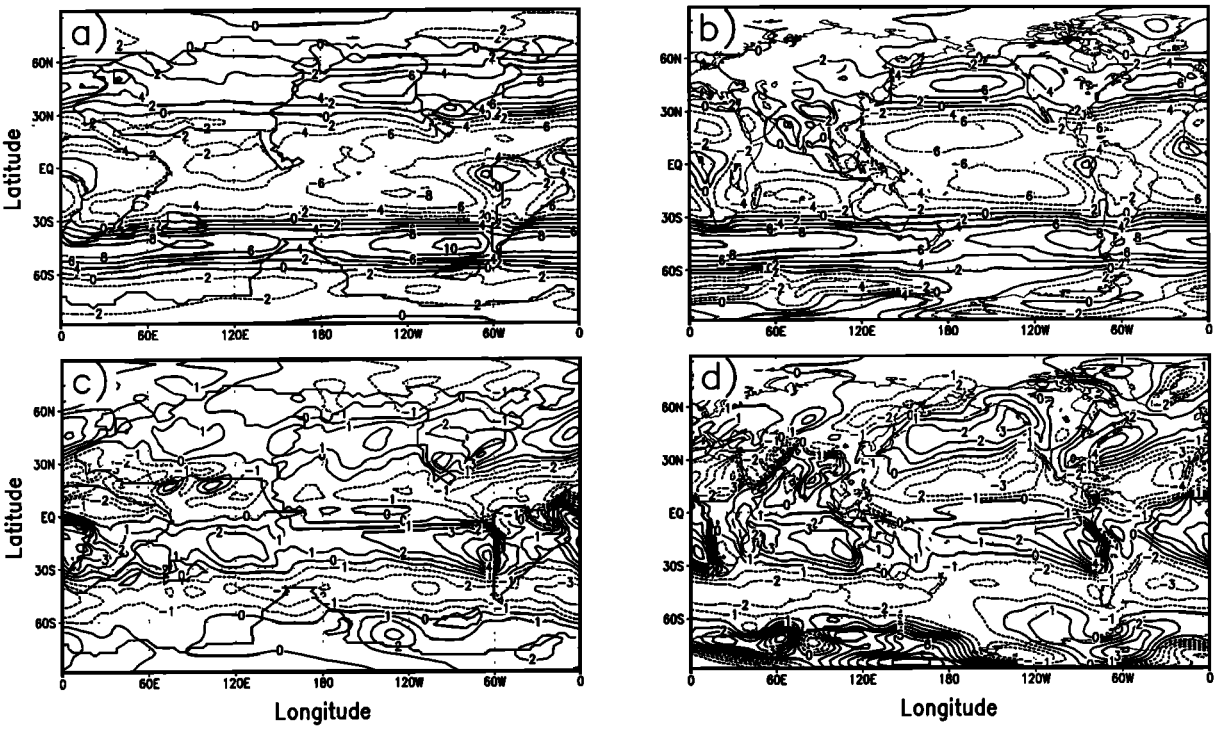

Figure 11. Annual mean $\sigma = 0.997$ components of horizontal velocity. Zonal and meridional velocities (in meters per second) for the Cretaceous are given in Figures 11a and 11c, respectively, and for the present day in Figures 11b and 11d, respectively. Contour intervals are 2 m/s for zonal velocity and 1 m/s for meridional velocity.

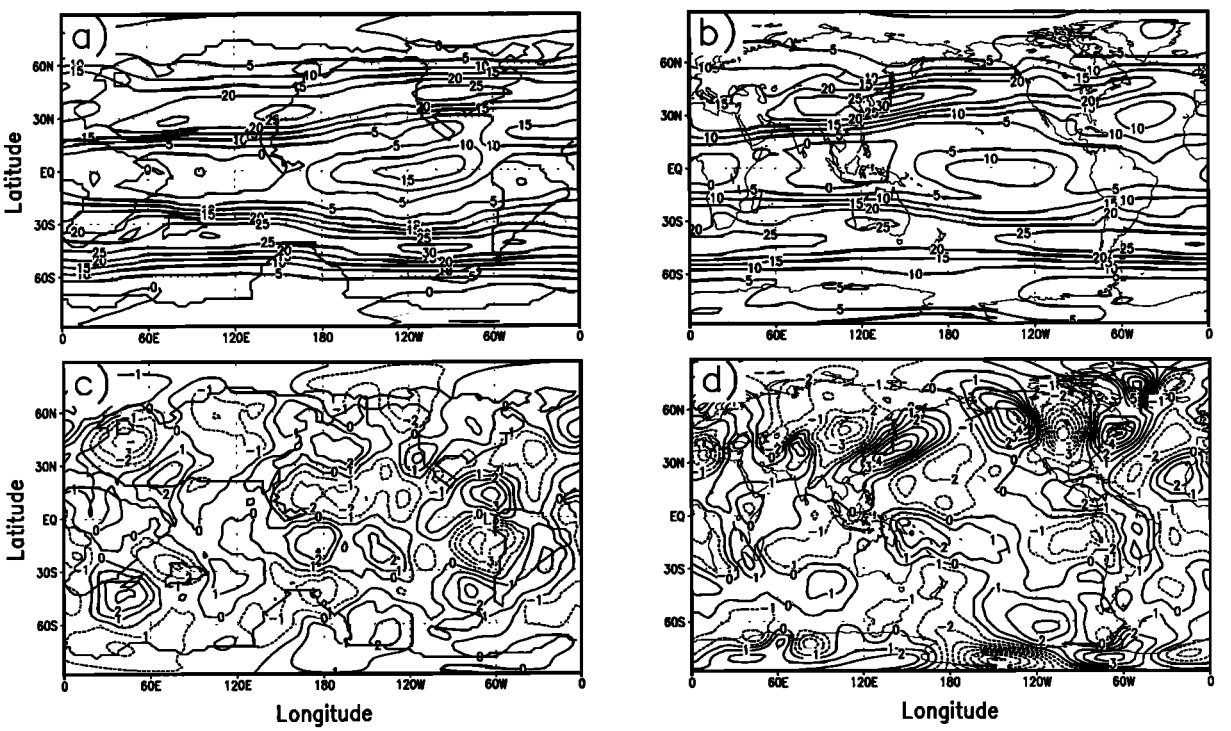

Figure 12. Same as Figure 11 but for the $\sigma = 0.355$ surface (upper troposphere). Contour intervals are 5 m/s for zonal velocity and 1 m/s for meridional velocity.

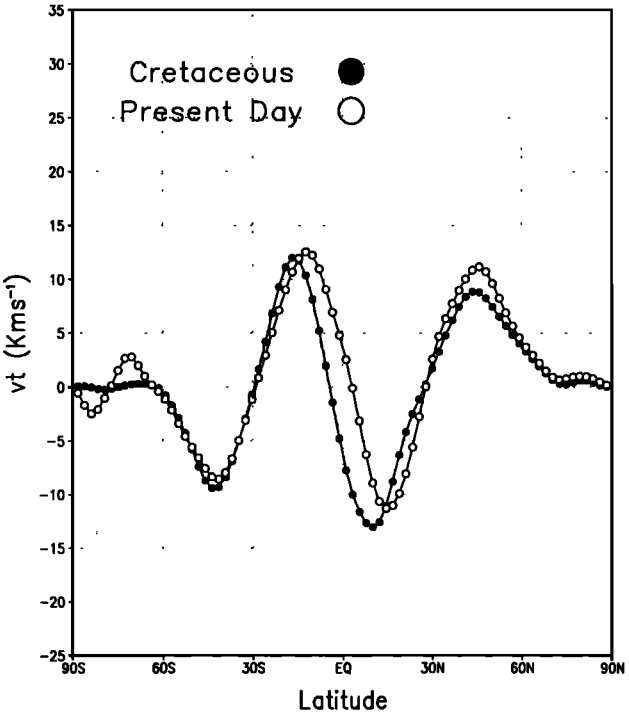

Figure 13. Annual mean, zonally and vertically averaged atmospheric poleward heat flux $\overline{V'T'}$ (as defined in text) for the Cretaceous (solid circles) and for the present day (open circles) simulations. Units are kelvins per meter per second (for units of 10^{15} W multiply by $2\pi R\cos\phi$, where R is the Earth's radius and ϕ is latitude).

ward winds over the western coasts of the warm South American and African continents (compare Figures 13c and 13d). The signature of midlatitude baroclinic eddy activity is evident as two strong maxima in poleward heat transport at 45°N and 45°S. The southern midlatitude transport in the Cretaceous is roughly the same as in the present day, whereas the northern midlatitude heat transport in the Cretaceous is reduced by approximately 3°K m/s. The lack of high topographical features in the Cretaceous northern hemisphere results in decreased eddy activity (as evident in the mean upper tropospheric meridional velocities of Figure 12c) and a reduced net heat flux, although within an individual baroclinic eddy the flux of latent heat will be greater in the Cretaceous as indicated by the increased midlatitude precipitation. In southern midlatitudes, where topographically induced eddies may only be triggered by the tail of the Andes in the present day, the net heat fluxes in the two simulations are comparable.

3.5. South Eurasian Monsoon

Despite the fact that the continental geometry and topography in the region bordering the north Indian Ocean are significantly different from those of today, a northern summer (JJA) monsoon flow develops along the southern edge of Cretaceous Eurasia (Figure 14). Since the monsoon winds are to first order a geostrophic phenomenon in balance with the spatial pattern of high and low pressures induced by the land-sea temperature differential, the main differences in the structure of the monsoon winds may be explained by differences in continental geometry. For example, in the present day the heat of the Indian subcontinent during the northern summer months induces cyclonic curvature to the flow over the Bay of Bengal (Figure 14b). In the Cretaceous the Indian subcontinent is an island in the southern subtropics and hence the cyclonic flow is absent. Additionally, strong southerly flow in the present-day monsoon results from the temperature-induced pressure differential between northeast Africa and the Arabian Sea (near 10°N; Figure 14b). In the Cretaceous the relatively cool water in the Tethys Seaway moderates the zonal pressure gradient in this region, and the southerly winds are thereby substantially weakened (Figure 14a).

The monsoon winds in the Cretaceous nevertheless bring large amounts of precipitation (~ 1.2 cm/d) to the Indonesian peninsula (Figure 15a). In the present climate, orographic uplift at the foothills of the Himalayan mountains induces a much larger amount of regional precipitation (Figure 15b), but those regions not as strongly affected by orography sustain rainfall rates similar to those in the Cretaceous simulation.

3.6. Upper Ocean

In response to the fourfold increase in atmospheric CO_2, Cretaceous mean SST increases rapidly over the first 20 years of the integration, stabilizing at a value that is ~5°C greater than that of the present day. The extratropical oceans poleward of 30°, which warm by ~5.2°C in the mean, contribute a majority of the warming and do not drop below freezing in the winter months: The minimum SST in the Arctic Ocean in January is 5.5°C and in the Antarctic Ocean in July it is 4.4°C . Equatorial SST increases by ~3.5°C and has a much shorter timescale of adjustment (~10 years). There is a 10°–15° poleward expansion of tropical SST (Figure 16), in agreement with the poleward shift in Cretaceous coral deposits [*Habicht*, 1979].

In a warm climate the high values of salinity that are required to initiate saline deep water formation are determined by net evaporative loss of fresh water to the atmosphere. The spatial locations of such regions are determined by the continental geometry and by the atmospheric temperature, wind speed, and precipitation. The annual mean surface salinity for the late Cretaceous (Figure 17a) indicates two regions of extremely high salinity (>38): the Gulf of Mexico and in the narrow strait between South America and Africa, where salinity reaches 38.5. Extensive salt deposits off the western

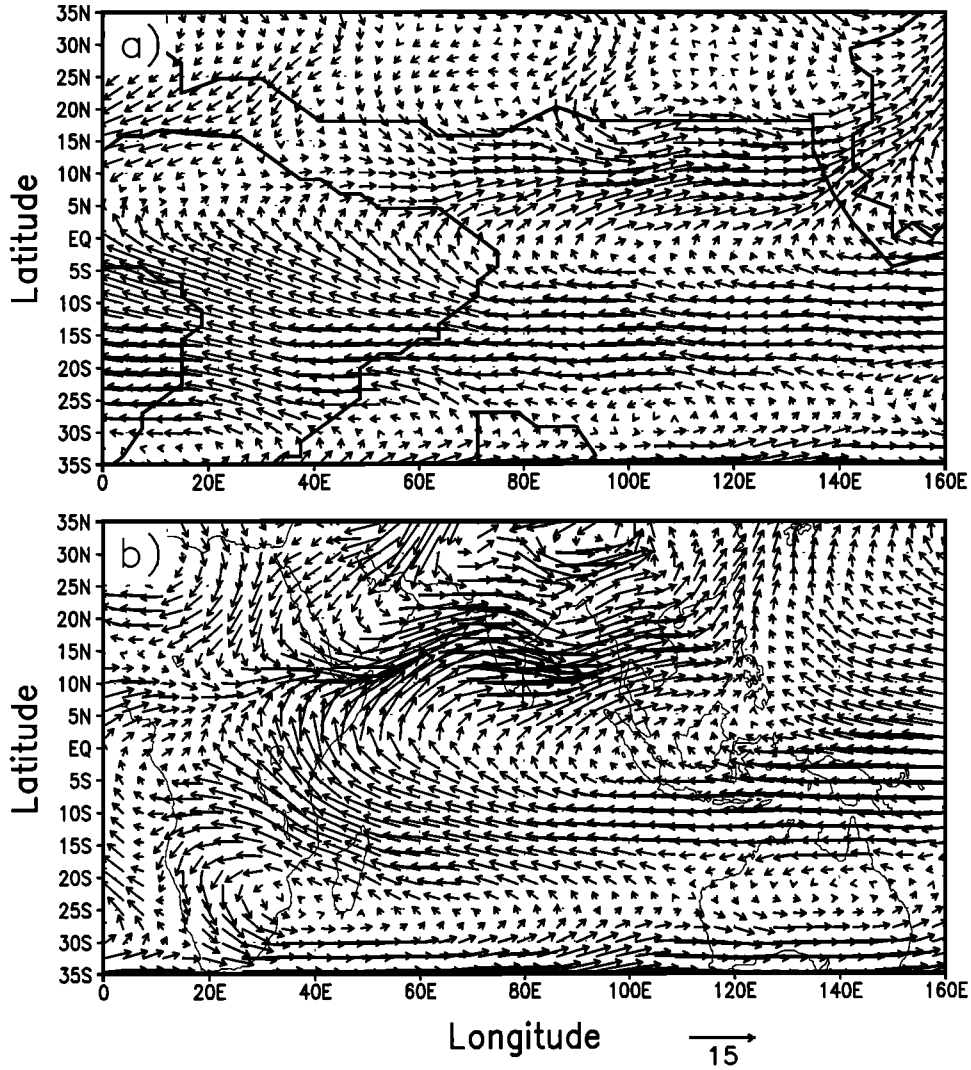

Figure 14. JJA horizontal winds in the south Asian monsoon region on the $\sigma = 0.866$ surface for (a) the Cretaceous and (b) the present day. Velocity vectors are scaled in both panels in meters per second as indicated in the bottom right.

coast of Africa and off the eastern coast of South America from the Cretaceous period [e.g., *Haq*, 1984] support the notion that the water between these continents was highly susceptible to salinification.

Increased zonal wind stress over the northern Pacific and Tethys Ocean basins increases the strength of the respective gyre circulations and of their western boundary currents by ~20%. The strengthened Pacific Walker cell increases the westward wind stress over the equatorial Pacific, thereby strengthening the Ekman divergence and its concomitant upwelling. Cretaceous analogues of the South Equatorial Current, the Equatorial Undercurrent, the Gulf Stream, the Kuroshio, and the Antarctic Circumpolar Current (ACC) all exist in the simulation (Figure 17b). It has been proposed that the development of the ACC requires two criteria to be satisfied: that the Drake Passage be open and that the Australian continent be separate from Antarctica [e.g., *Crowley and North*, 1991]. The existence of an ACC in our simulation demonstrates that a circumpolar current is possible even when the northernmost end of the Australian continent extends to 40°S, as is the case in this experiment.

The most unique feature of the wind-driven circulation is a westward circumglobal current, the Tethys Circumglobal Current (TCC), which exists at the surface with a depth that varies from ~350 m in the Tethys Seaway to ~100 m in the Pacific basin. The simulated TCC is not interrupted seasonally by the surface current reversals in the Tethys Seaway induced by the south Eurasian monsoon [*Bush*, 1997]. Nevertheless, the eastward monsoon current induces seasonal upwelling along the northern Tethys region and may account for the upwelling inferred from siliceous deposits [*Blueford*, 1988].

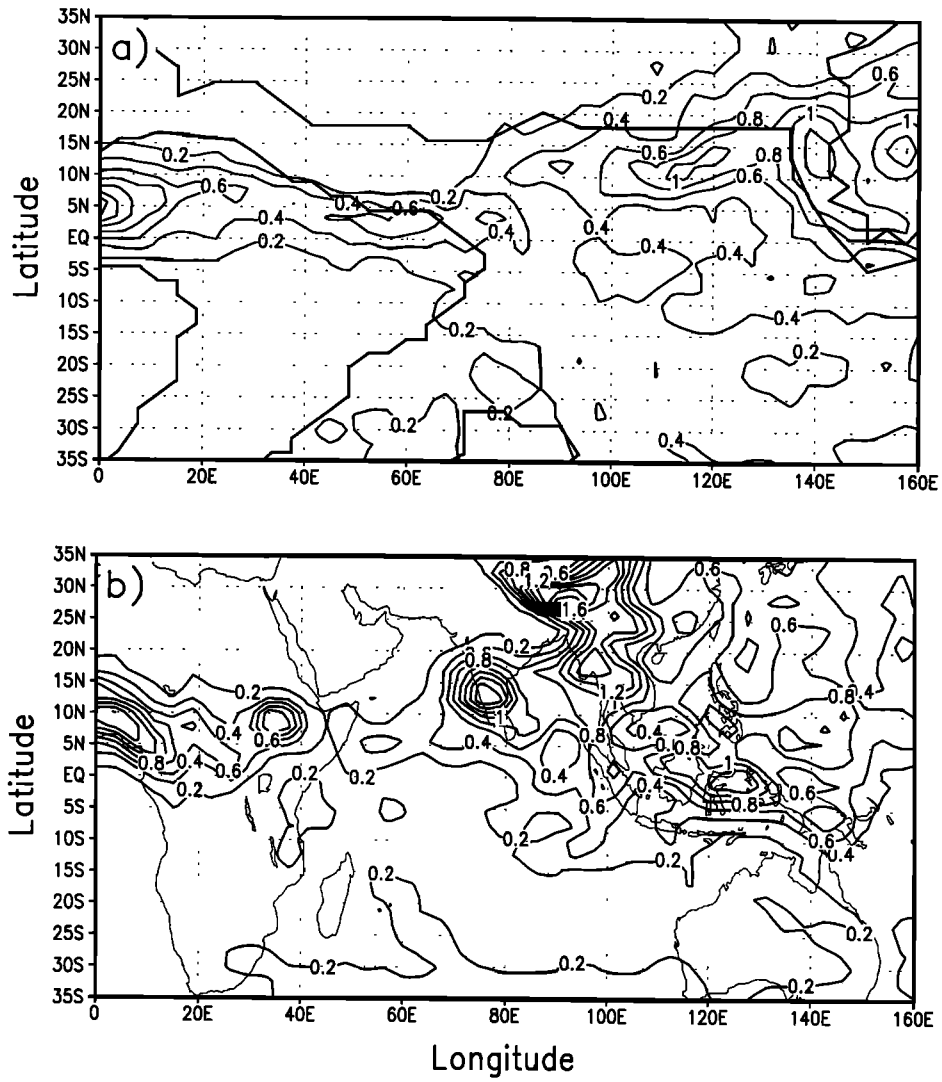

Figure 15. JJA precipitation in the south Asian monsoon region for (a) the Cretaceous and (b) the present day. The contour interval is 0.2 cm/d in both panels.

Southwestward flow of the TCC along the northwestern coast of Africa induces local coastal upwelling and cold SST in the simulation (compare Figure 16). Evidence for such upwelling along the Moroccan coast has been presented by *Haq* [1984]. The presence of shallow, epicontinental seas, however, would affect the structure of the TCC, particularly over north Africa. Recirculation gyres in the shallow sea would be likely. However, there is substantial westward mass transport into the region from the Indian Ocean, a transport that is driven by the easterly trade winds whose direction would not be different if a shallow sea were included. We would therefore expect, by continuity, a large transport out of the Tethys Seaway into the Tethys Ocean, although the structure of the current system in the seaway itself might be quite complex.

4. Discussion

It has been demonstrated by *Hansen et al.* [1984] that altered continental geography and differing land vegetation (hence albedo) play a secondary role to CO_2 in terms of global temperature modification. Hence we may hold the fourfold increase in atmospheric CO_2 responsible for the majority of the increase in temperature and moisture of the simulated Cretaceous climate. As the SST is predicted in the coupled model according to both thermodynamics and hydrodynamics, the dominant surface boundary forcing of the atmosphere by the ocean is consistent with the predicted climate. The Cretaceous atmospheric temperature exhibits a global increase of $\sim 4°$K over that of the present day, with a majority of the increase occurring in the lower tropo-

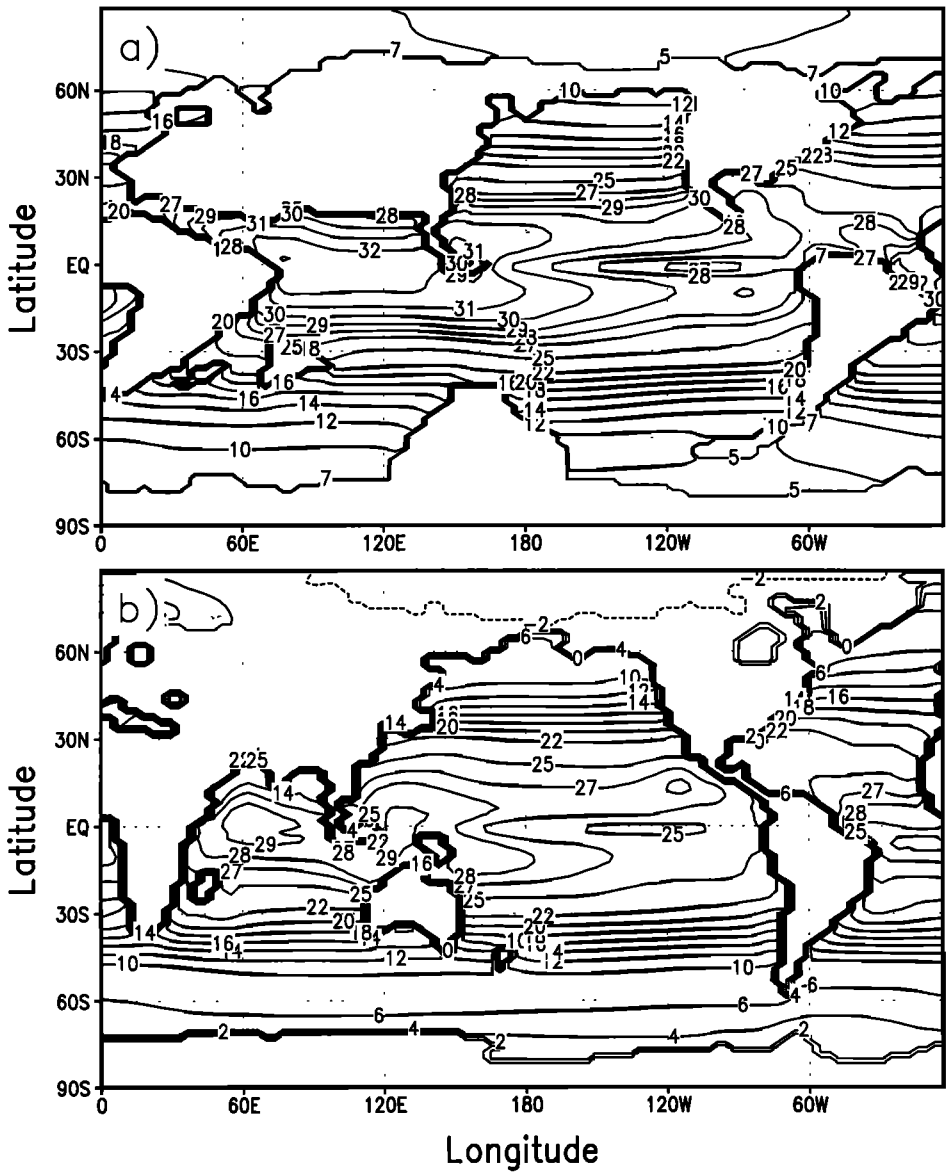

Figure 16. Spatial distribution of annual mean SST (°C) for (a) the Cretaceous and (b) the present day. Contours are in degrees centigrade.

sphere in high latitudes. Although tropical temperatures increase by ~5°K , they are not sufficiently high to maintain the present linear equator-to-pole surface temperature gradient given the high-latitude warming. The zonally averaged surface temperature profile that emerges from the simulation is in good agreement with profiles derived from proxy data and presented by *Barron* [1983] as bounds on the surface temperature during the Cretaceous. The spatial distribution of surface temperature is quite similar to that arising from simulations of the mid-Cretaceous which included both topography and reduced land area [*Barron and Washington*, 1984]. A simulated $10°-15°$ poleward expansion of tropical sea surface temperatures is also in good agreement with the latitudinal shift in coral deposits from this period [*Habicht*, 1979].

The linear equator-to-pole temperature gradient in the Cretaceous is therefore indicative of an "equable" climate near the surface, despite the fact that the mid-latitude temperature gradient is similar to that of the present day. This suggests that the spatial location of proxy data points is a crucial factor if mean global temperature gradients are to be inferred.

Nevertheless, the reduced surface meridional temperature gradient in the atmosphere does not persist in the vertical. Middle to upper troposphere baroclinicity remains approximately the same as the present day's (compare Figure 6). The simulated Cretaceous midlat-

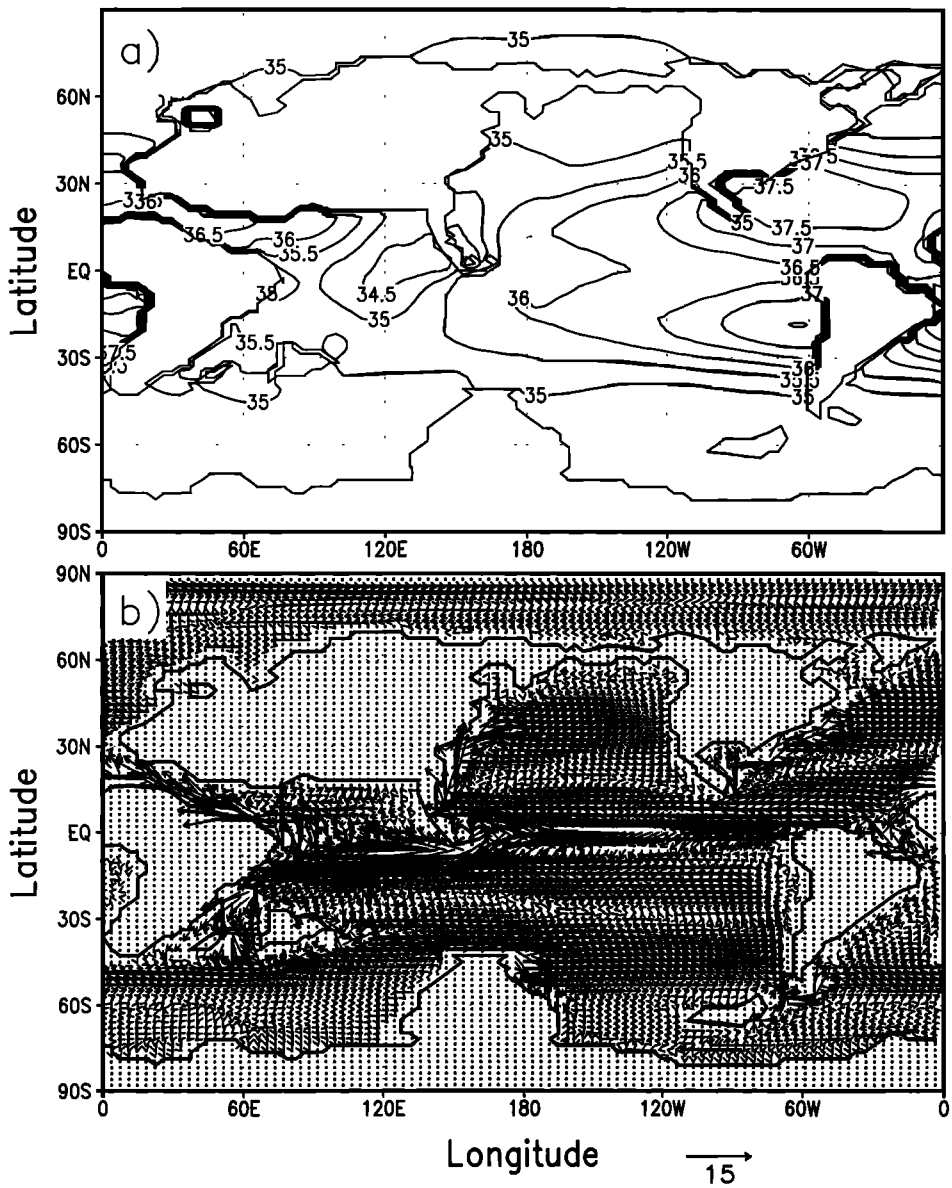

Figure 17. (a) Annual mean sea surface salinity for the late Cretaceous (the contour interval is 0.5). (b) Annual mean ocean velocity vectors at a depth of 52 m (to remove the Ekman velocity component; vectors are scaled in units of centimeters per second as shown in the figure).

itude jets are therefore comparable in size and strength to those of the present day and are quite similar to those that arise in atmosphere-only integrations with present-day ocean heat transport imposed [*Barron et al.*, 1993]. These results suggest that while equable conditions may exist in surface temperature (and would hence be reflected in the proxy data), they do not necessarily exist at middle-upper tropospheric height. This point has been noted previously by *Barron and Washington* [1982] in atmospheric GCM calculations which incorporated a mixed-layer ocean model. It is of special interest in the present study because it implies that the winds, which drive the ocean's surface currents through mechanical forcing and which produce the convergent and divergent zones which regulate buoyancy forcing, are not reduced, and hence the wind-driven ocean circulation is as vigorous as it is in the present day. In fact, the slightly stronger surface atmospheric winds in this Cretaceous simulation drive an even stronger ocean circulation despite the fact that the surface temperature is more equable in a linear sense. Nevertheless, it is possible that different orbital parameters might affect the vertical structure of the meridional temperature gradient through, for example, increased seasonality.

The increased temperatures of the Cretaceous imply an increase in the saturation vapor pressure of the atmosphere. The magnitude of convergence of surface winds in, for example, the ITCZ remains approximately the same as today (although the location is more equatorward; Figures 7, 11c, and 11d). Increased atmospheric moisture content therefore implies an increase in precipitation and latent heat release in the tropical convergence zones and in midlatitude baroclinic eddies. The warm temperatures and increased precipitation simulated in the midlatitudes are consistent with the substantial coal deposits that were formed in these regions during the Cretaceous period [*Parrish et al.*, 1982]. The equatorward shift of the northern hemisphere Hadley cells is also reflected in the geological record's distribution of Mesozoic evaporites [*Gordon*, 1975; *Parrish et al.*, 1982]. This mean shift is attributed to the equatorward displacement of the ITCZ over the Pacific Ocean, particularly in the eastern Pacific where strong northeasterly winds flow between the separated North and South American continents (compare Figure 11). We note an ~20% increase in strength of the north equatorial Hadley cell and an ~20% decrease in strength of the south equatorial Hadley cell. In comparison with the global increase in strength of the Hadley circulation observed by *Manabe and Bryan* [1985] for an increased CO_2 experiment for present-day geography, we conclude that continental boundary forcing (e.g., glacial ice, continental repositioning, topography, and the resulting changes in number and strength of midlatitude baroclinic eddies) plays a fundamental role in the strength of this circulation and can dominate changes induced by a quadrupling of CO_2.

The Walker circulation of the Cretaceous simulation, which exhibits a stronger and zonally broader Pacific Walker cell, suggests that the equatorial easterlies were stronger than in the present day. These easterlies induce poleward Ekman divergence in the upper ocean and concomitant equatorial upwelling. Siliceous deposits from the Cretaceous equatorial Pacific [*Drewry et al.*, 1974] do indeed indicate the presence of upwelling in this region (although we cannot determine its relative strength).

A south Eurasian monsoon circulation exists in the late Cretaceous simulation, but it is quite different from that of today's climate. The main differences are attributed to the altered continental geometry of the late Cretaceous period. First, the absence in the region of the Indian subcontinent itself makes the Cretaceous monsoon more zonal over the eastern Indian Ocean. Second, the presence of the ocean-filled Tethys Seaway between Africa and Eurasia moderates the zonal pressure gradient in the region and weakens the southerly monsoon winds off the east African coast. In the present day these southerly winds form the strong Somali jet which is the source of much of the monsoon's moisture. A reduction of these winds in the Cretaceous decreases the availabe moisture and precipitation in the monsoon (compare Figure 10). However, regional topography would obviously have an impact on the Eurasian monsoon. Growth of the Himalayan mountain chain was initiated when India collided with Eurasia ~50 Ma, was most rapid in the mid-Eocene to early Miocene, and finally attained present elevations at ~8 Ma in the late Miocene [e.g., *Windley*, 1995]. Such high mountains increase the inland penetration of the monsoon jet and increase regional precipitation [e.g., *Hahn and Manabe*, 1975]. Although these mountains were absent during the Cretaceous, other topographical features in the region may have been high enough to impact the strength of this monsoon and its related oceanic current. This question will be explored in a future sensitivity study.

The reduced amount of seasonal snow and ice in the Cretaceous simulation implies a decrease in ice-albedo feedback in high latitudes. The amplitude of the seasonal cycle in temperature is decreased by approximately 10% over eastern Eurasia and by nearly 30% over North America. The freezing line in the northern hemisphere (i.e., the latitude poleward of which seasonal temperatures drop below freezing) shifts poleward by anywhere from 5° in coastal areas to 45° over western Eurasia. The latter shift is due in part to the regional warming induced by the subtropical diversion of the warm, saline TCC as well as to the increased strength of the Cretaceous Gulf Stream. These results indicate that as in the present climate, wind-driven ocean features such as western boundary currents and equatorial currents play a significant role in determining the surface temperature distribution. This point was also noted by *Barron et al.* [1993] in their GCM calculations with specified ocean heat transport. Nevertheless, if the definition of equable is taken to mean an absence of even seasonal freezing temperatures in the continental interiors then an equable climate is not realized in this simulation and, as first proposed by *Sloan and Barron* [1990], the concept of an equable Cretaceous climate needs serious reconsideration.

In fact, recent evidence for eustatic sea level fluctuations in the Cretaceous which are linked to glaciation [*Stoll and Schrag*, 1996] suggest that cold high-latitude temperatures may be quite realisitic in simulations of the Cretaceous climate. While the annual mean temperature over Antarctica is below zero in our simulation (compare Figure 4), no year-round freezing temperatures are present and therefore no glaciation would be possible. However, given a simulated maximum January temperature of 8°C near the south pole (compare Figure 5a) and a dry adiabatic lapse rate of ~10°K/km, temperatures are below freezing year-round at an altitude of only 800 m. If topography of this height

were included over Antarctica, however, the freezing level would rise in response to surface heating from the imposed topography itself. It remains at present unclear just how high topography should be in this region to permit glaciation. Additionally, recent GCM sensitivity studies have demonstrated a higher sensitivity of summer snow cover to a 3% decrease in solar luminosity than to variations in topographic height [*Otto-Bliesner*, 1996]. While we have kept the solar constant at its present value in the Cretaceous simulation, evolution of solar luminosity [*Endal and Sofia*, 1981] suggests that for 65 Ma the solar constant may have been smaller by upward of 1% which produces, according to energy balance models, an $\sim 1^{\circ}$C reduction in global temperature [e.g., *Crowley and North*, 1991].

Such intriguing questions lead us to list some caveats concerning interpretation of these results. As with all atmosphere and ocean GCMs currently in existence, coupled climate models do not exactly reproduce every feature of the present climate. However, the robust features of the general circulation such as the trade winds, the monsoons, the ITCZ, and the wind-driven ocean currents are quite well simulated for the present-day. An attempt has therefore been made in this study to compare our model results for the Cretaceous to the present-day simulation and, when possible, to available proxy data. In general, the model does well in simulating the enhanced midlatitude precipitation, the equatorward shift of the northern subtropical high, the poleward expansion of tropical SST, and the easterly equatorial trade winds that have been inferred from the geological record. Nevertheless, our exclusion of Cretaceous topography most likely overestimates the amount of precipitation over those continental interiors that were bordered by steep mountains and may underestimate the strength of the south Eurasian monsoon. Shallow inland seas may have moderated the amplitude of the seasonal cycle even further than has been simulated here (compare Figure 5), and they may have been large enough to affect global temperature through reduction of the planetary albedo. The CO_2 levels imposed in this experiment do not significantly alter the dynamical structure of the tropospheric circulation (see Figure 6) although they do increase global temperature. Higher values of CO_2 would produce an even warmer, wetter climate, and lower values would produce a cooler, drier climate. Imposition of present-day orbital parameters prescribes the latitudinal distribution of incoming radiative forcing and gives us a first guess at the ocean's meridional SST structure. It is probable that the mean meridional gradients that we observe in the atmosphere and the ocean would be different if a variation in the orbital parameters were to be made. Nevertheless, further sensitivity studies with the coupled model are required in order to assess the impact of changing orbital parameters on the coupled system.

5. Conclusions

We have presented results for the climate of the late Cretaceous as delivered from integration of a coupled atmosphere-ocean GCM and have compared them with those of a present-day control simulation and to available proxy data. Forcing parameters of the atmosphere-ocean system that have been altered in the Cretaceous simulation are atmospheric CO_2 (which we quadruple), continental geometry (which is taken from late Cretaceous paleobiogeographic reconstructions), and surface albedo.

Higher levels of atmospheric CO_2 result in a global temperature increase of 4°K (the majority of which occurs in the lower troposphere at high latitudes) and a $10^{\circ}-15^{\circ}$ poleward shift of the atmospheric and oceanic tropical zones. The increase in SST is most prominent in high latitudes, where the magnitude of the increase is such that the minimum winter SST is $\sim 4^{\circ}-5^{\circ}$C . The global warming precludes existence of the permanent Antarctic and Greenland ice sheets of the present climate if no topographic height is included, as is the case for this experiment. The warming increases the atmospheric saturation vapor pressure, increasing latent heat release and global precipitation by 10% . Elimination of the ice sheets reduces the near-surface equator-to-pole temperature gradient but does not reduce the middle to upper tropospheric baroclinicity. Hence the midlatitude jets and the mechanical forcing of the ocean circulation are not reduced, and an $\sim 20\%$ increase in strength of the gyre circulations is realized. The conjecture of a weaker ocean circulation in a climate which exhibits a weaker linear pole-to-equator surface temperature gradient is therefore not supported by this simulation.

The amplitude of the seasonal cycle in temperature is decreased as a result of the elimination of year-round snow and ice with their concomitant albedo feedback. Nevertheless, there are continental regions in the Cretaceous that seasonally drop below freezing. If the definition of equable is taken to mean a complete absence of freezing temperatures then we conclude that even with ocean dynamics explicitly calculated, an equable climate by that definition does not exist in the parameter range that we have investigated.

Changes in the large-scale Hadley circulation induced by the altered boundary forcing of the Cretaceous environment result in weaker southern hemisphere and stronger northern hemisphere cells. With an $\sim 6^{\circ}$ equatorward shift of the northern hemisphere cells, the mean meridional circulation becomes much more symmetric about the equator. A substantial increase in the Pacific Walker circulation in the late Cretaceous can be linked to the increased strength of convection over the western Pacific and to the separation of the North and South American continents. The zonal extent of the Pacific Walker cell increases in the Cretaceous as a re-

sult of the increased width of the Pacific basin. These large-scale winds drive a vigorous wind-driven ocean circulation which exhibits Cretaceous analogues of all the major modern currents in addition to the unique TCC.

Acknowledgments. The authors thank Eric Barron and Lisa Sloan for very helpful comments on a previous version of this manuscript. A.B.G.B. gratefully acknowledges the support of a PDF through UCAR's Visiting Science Program.

References

Barron, E.J., A warm, equable Cretaceous: The nature of the problem, *Earth Sci. Rev., 19*, 305-338, 1983.

Barron, E.J., Tropical climate stability and implications for the distribution of life, in *Effects of Past Global Change on Life*, Studies in Geophysics, National Research Council, 250 pp., National Acad. Press, Washington, D. C., 1995.

Barron, E.J., and W.H. Peterson, Model simulation of the Cretaceous ocean circulation, *Science, 244*, 684-686, 1989.

Barron, E.J., and W.H. Peterson, Mid-Cretaceous ocean circulation: Results from model sensitivity studies, *Paleoceanogr., 5*, 319-337, 1990.

Barron, E.J., and W. Washington, The atmospheric circulation during warm, geologic periods: Is the equator-to-pole surface temperature gradient the controlling factor?, *Geology, 10*, 533-636, 1982.

Barron, E.J., and W. Washington, The role of geographic variables in explaining paleoclimates: Results from Cretaceous climate model sensitivity studies, *J. Geophys. Res., 89*, 1267-1279, 1984.

Barron, E.J., and W. Washington, Warm Cretaceous climates: High atmospheric CO_2 as a plausible mechanism, in *The Carbon Cycle and Atmospheric CO_2: Natural Variations Archean to Present, Geophys. Monogr. Ser.*, vol. 32, edited by E.T. Sundquist and W.S. Broecker, pp. 546-553, AGU, Washington, D. C., 1985.

Barron, E.J., S.L. Thompson, and S.H. Schneider, An ice-free Cretaceous? Results from climate model simulations, *Science, 212*, 501-508, 1981.

Barron, E.J., W.H. Peterson, D. Pollard, and S. Thompson, Past climate and the role of ocean heat transport: Model simulations for the Cretaceous, *Paleoceanography, 8*, 785-798, 1993.

Berner, R.A., A model for atmospheric CO_2 over Phanerozoic time, *Am. J. Sci., 291*, 339-376, 1991.

Blueford, J.R., Radiolarian evidence: Late Cretaceous through Eocene ocean circulation patterns, in *Siliceous Deposits of the Tethys and Pacific Regions*, edited by J.R. Hein and J. Obradovic, pp. 19-29, Springer-Verlag, New York, 1988.

Brass, G.W., J.R. Southam, and W.H. Peterson, Warm saline bottom water in the ancient ocean, *Nature, 296*, 620-623, 1982.

Brenchley, P.J. (Ed.), *Fossils and Climate*, 352 pp., John Wiley, New York, 1984.

Broccoli, A.J., and S. Manabe, The effects of orography on midlatitude northern hemisphere dry climates, *J. Clim., 5*, 1181-1201, 1992.

Brouwers, E.M., W.A. Clemens, R.A Spicer, T.A. Ager, L.D. Carter, and W.V. Sliter, Dinosaurs on the North Slope, Alaska: High latitude, latest Cretaceous environments, *Science, 237*, 1608-1610, 1987.

Bryan, K., A numerical method for the study of the circulation of the world ocean, *J. Comput. Phys., 3*, 347-376, 1969.

Bush, A.B.G., Numerical simulation of the Cretaceous Tethys Circumglobal Current, *Science, 275*, 807-810, 1997.

Cerling, T.E., Carbon dioxide in the atmosphere: Evidence from Cenozoic and Mesozoic paleosols, *Am. J. Sci., 291*, 377-400, 1991.

Crowley, T.J., and G.R. North, *Paleoclimatology, Oxford Monogr. on Geol. and Geophys. 18*, 339 pp., Oxford University Press, New York, 1991.

Crowley, T.J., J.G. Mengel, and D.A. Short, Gondwanaland's seasonal cycle, *Nature, 329*, 803-807, 1987.

Crowley, T.J., W.T. Hyde, and D.A. Short, Seasonal cycle variations on the supercontinent of Pangaea, *Geology, 17*, 457-460, 1989.

Drewry, G.E., A.T.S. Ramsay, and A.G. Smith, Climatically controlled sediments, the geomagnetic field and trade wind belts in Phanerozoic time, *J. Geol., 82*, 531-553, 1974.

Endal, A.S., and S. Sofia, Rotation in solar-type stars, I, Evolutionary models for the spindown of the Sun, *Astrophys. J., 243*, 625-640, 1981.

Gordon, W.A., Distribution by latitude of Phanerozoic evaporite deposits, *J. Geol., 83*, 671-684, 1975.

Gordon, C.T., and W. Stern, A description of the GFDL global spectral model, *Mon. Weather Rev., 110*, 625-644, 1982.

Habicht, J.K.A., *Paleoclimate, Paleomagnetism, and Continental Drift*, Am. Assoc. Petrol. Geol. Stud. Geol., no. 9, Tulsa, Okla., 1979.

Hahn, D.G., and S. Manabe, The role of mountains in the south Asian monsoon circulation, *J. Atmos. Sci., 32*, 1515-1541, 1975.

Hansen, J.E., A. Lacis, D. Rind, G. Russell, P. Stone, I. Fung, R. Ruedy, and J. Lerner, Climate sensitivity: Analysis of feedback mechanisms, in *Climate Processes and Climate Sensitivity, Geophys. Monogr. Ser.*, vol. 29, edited by J.E. Hansen and T. Takahashi, pp. 130-163, AGU, Washington, D. C., 1984.

Haq, B.U., Paleoceanography: A synoptic overview of 200 million years of ocean history, in *Marine Geology and Oceanography of Arabian Sea and Coastal Pakistan*, edited by B.U. Haq and J.D. Milliman, pp. 201-231, Van Nostrand Reinhold, New York, 1984.

Kondratyev, K.Y., *Radiation in the Atmosphere*, 912 pp., Academic, San Diego, Calif., 1969.

Lasaga, A.C., R.A. Berner, and R.M. Garrels, An improved geochemical model of atmospheric CO_2 fluctuations over the past 100 million years, in *The Carbon Cycle and Atmospheric CO_2: Natural Variations Archean to Present, Geophys. Monogr. Ser.*, vol. 32, edited by E.T. Sundquist and W.S. Broecker, pp. 397-411, AGU, Washington, D. C., 1985.

Levitus, S., Climatological atlas of the world ocean, *NOAA Prof. Paper 13*, 173 pp., U.S. Govt. Print. Office, Washington, D. C., 1982.

Luyendyk, B.P., D. Forsyth, and J.D. Phillips, Experimental approach to the paleocirculation of the oceanic surface waters, *Geol. Soc. Am. Bull., 83*, 2649-2664, 1972.

Manabe, S., and K.B. Bryan Jr., CO_2-induced change in a coupled ocean-atmosphere model and its paleoclimatic implications, *J. Geophys. Res., 90*, 11,689-11,707, 1985.

Manabe, S., and R.J. Stouffer, Simulation of abrupt climate change induced by freshwater input to the North Atlantic Ocean, *Nature, 378*, 165-167, 1995.

Otto-Bliesner, B.L., Initiation of a continental ice sheet in a global climate model (GENESIS), *J. Geophys. Res., 101*, 16,909-16,920, 1996.

Pacanowski, R.C. and S.G.H. Philander, Parameterization

of vertical mixing in numerical models of tropical oceans, *J. Phys. Oceanogr., 11*, 1443-1451, 1981.

Pacanowski, R.C., K. Dixon, and A. Rosati, *The GFDL modular ocean model user guide, GFDL Ocean Group Tech. Rep. 2*, Geophys. Fluid Dyn. Lab., Princeton, N. J., 1991.

Parrish, J.T., and R.A. Spicer, Late Cretaceous terrestrial vegetation: A near-polar temperature curve, *Geology, 16*, 22-25, 1988.

Parrish, J.T., A.M. Ziegler, and C.R. Scotese, Rainfall patterns and the distribution of coals and evaporites in the Mesozoic and Cenozoic, *Palaeogeogr. Palaeoclimatol. Palaeoecol., 40*, 67-101, 1982.

Peixoto, J.P., and A.H. Oort, *Physics of Climate*, 520 pp., Am. Inst. of Phys., New York, 1992.

Philander, S.G.H., D. Gu, D. Halpern, G. Lambert, N.-C. Lau, T. Li, and R.C. Pacanowski, Why the ITCZ is mostly north of the equator, *J. Clim., 9*, 2958-2972, 1995.

Rau, G.H., T. Takahashi, and D.J. Des Marais, Latitudinal variations in plankton $\delta^{1}3C$: Implications for CO_2 and productivity in past oceans, *Nature, 341*, 516-518, 1989.

Rich, P.V., T.H. Rich, B.E. Wagstaff, J. McEwen Mason, C.B. Douthitt, R.T. Gregory, E.A. Felton, Evidence for low temperatures and biologic diversity in Cretaceous high latitudes of Australia, *Science, 242*, 1403-1406, 1988.

Sandberg, P.A., An oscillating trend in Phanerozoic nonskeletal carbonate mineralogy, *Nature, 305*, 19-22, 1983.

Savin, S.M., The history of the Earth's surface temperature during the past 100 million years, *Ann. Rev. Earth Planet. Sci., 5*, 319-355, 1977.

Sloan, L.C., and E.J. Barron, "Equable" climates during Earth history?, *Geology, 18*, 489-492, 1990.

Smiley, C.J., Paleoclimatic interpretations of some Mesozoic floral sequences, *Am. Assoc. Pet. Geol. Bull., 51*, 849-863, 1967.

Stoll, H.M., and D.P. Schrag, Evidence for glacial control of rapid sea level changes in the early Cretaceous, *Science, 272*, 1771-1774, 1996.

Stone, H.M. and S. Manabe, Comparisons among various numerical models for computing infrared cooling, *Mon. Weather Rev., 96*, 735-741, 1968.

Washington, W.M., and G.A. Meehl, Seasonal cycle experiment on the climate sensitivity due to a doubling of CO_2 with an atmospheric general circulation model coupled to a simple mixed-layer ocean model, *J. Geophy. Res., 89*, 9475-9503, 1984.

Wetherald, R.W., and S. Manabe, Cloud feedback processes in a general circulation model, *J. Atmos. Sci., 45*, 1397-1415, 1988.

Windley, B.F., *The Evolving Continents*, 3rd ed., 526 pp., John Wiley, New York, 1995.

Wolfe, J.A., and G.R. Upchurch, North American nonmarine climates and vegetation during the late Cretaceous, *Palaeogeogr. Palaeoclimatol. Palaeoecol., 61*, 33-77, 1987.

Ziegler, A.M., M.L. Hulver, A.L. Lottes, and W.F. Schmachtenberg, Uniformitarianism and palaeoclimates: Inferences from the distribution of carbonate rocks, in *Fossils and Climate*, edited by P.J. Brenchley, pp. 3-25, John Wiley, New York, 1984.

A. B. G. Bush, 126 Earth Sciences Building Department of Earth and Atmospheric Sciences, University of Alberta, Edmonton, Alberta, Canada T6G 2E3. (email: bush@mercury.geog.ualberta.ca)

S. G. H. Philander, Program in Atmospheric and Oceanic Sciences, P.O. Box CN710, Sayre Hall, Princeton University, Princeton, New Jersey, USA 08544-0710. (e-mail: gphlder@splash.princeton.edu)

(Received July 8, 1996; revised February 26, 1997; accepted March 10, 1997.)